Redox Biology 38 (2021) 101789

Contents lists available at ScienceDirect

Redox Biology

journal homepage: www.elsevier.com/locate/redox

Research Paper

Protective role of microglial HO-1 blockade in aging: Implication of iron metabolism

Cristina Fernández-Mendívil [a,b], Enrique Luengo [a,b], Paula Trigo-Alonso [a,b], Nuria García-Magro [c], Pilar Negredo [c], Manuela G. López [a,b,*]

[a] Instituto Teófilo Hernando for Drug Discovery. Department of Pharmacology. School of Medicine. Universidad Autónoma Madrid. Madrid, Spain
[b] Instituto de Investigación Sanitario (IIS-IP), Hospital Universitario de La Princesa, Madrid, Spain
[c] Department of Anatomy, Histology and Neuroscience. School of Medicine. Universidad Autónoma de Madrid. Madrid, Spain

ARTICLE INFO

Keywords:
Heme oxygenase-1
Microglia
Neuroinflammation
Iron metabolism
Ferroptosis
Aging

ABSTRACT

Heme oxygenase-1 (HO-1) is an inducible enzyme known for its anti-inflammatory, antioxidant and neuroprotective effects. However, increased expression of HO-1 during aging and age-related neurodegenerative diseases have been associated to neurotoxic ferric iron deposits. Being microglia responsible for the brain's innate immune response, the aim of this study was to understand the role of microglial HO-1 under inflammatory conditions in aged mice. For this purpose, aged wild type (WT) and LysMCreHmox1$^{\triangle\triangle}$ (HMOX1$^{M\text{-}KO}$) mice that lack HO-1 in microglial cells, were used. Aged WT mice showed higher basal expression levels of microglial HO-1 in the brain than adult mice. This increase was even higher when exposed to an inflammatory stimulus (LPS via i.p.) and was accompanied by alterations in different iron-related metabolism proteins, resulting in an increase of iron deposits, oxidative stress, ferroptosis and cognitive decline. Furthermore, microglia exhibited a primed phenotype and increased levels of inflammatory markers such as iNOS, p65, IL-1β, TNF-α, Caspase-1 and NLRP3. Interestingly, all these alterations were prevented in aged HMOX1$^{M\text{-}KO}$ and WT mice treated with the HO-1 inhibitor ZnPPIX. In order to determine the effects of microglial HO-1-dependent iron overload, aged WT mice were treated with the iron chelator deferoxamine (DFX). DFX caused major improvements in iron, inflammatory and behavioral alterations found in aged mice exposed to LPS. In conclusion, this study highlights how microglial HO-1 overexpression contributes to neurotoxic iron accumulation providing deleterious effects in aged mice exposed to an inflammatory insult.

1. Introduction

Aging is one of the main risk factors for the development of neurodegenerative diseases (NDDs). As life expectancy expands, the incidence of NDDs in the population increases, leading to an important socioeconomic impact [1–3]. Therefore, a deeper understanding of the pathogenesis of NDDs is required to identify new therapeutic targets. NDDs share common pathological mechanisms, which are also characteristic of aging, such as a low-grade inflammation, oxidative stress (OS), mitochondrial dysfunction, or protein aggregation [4–6]. Related to inflammation, it has been reported that inflammatory challenges in the periphery of the elder population are linked to inflammation in the brain, activation of microglia, synaptic dysfunction, neuronal death and cognitive decline; thus, prompting the development of NDDs [3,7–9].

Microglia comprise approximately 6–12% of all the cells found in the

Abbreviations: AD, Alzheimer's disease; ANOVA, analysis of variance; CD163, cluster of differentiation 163; CNS, central nervous system; CO, carbon monoxide; DFX, deferoxamine; DHE, dihydroethydium; DMT1, divalent metal transporter 1; EAE, experimental autoimmune encephalomyelitis; Fn, ferritin; FPN1, ferroportin 1; GPX4, glutathione peroxidase 4; Hb, hemoglobin; HCT, hematocrit; H_2DCFDA, 2′,7′-dichlorodihydrofluorescein diacetate; HO-1, heme oxygenase 1; IL-1β, interleukin 1 beta; iNOS, inducible nitric oxide synthase; LPS, lipopolysaccharide; MCV, mean corpuscular volume; NDD, neurodegenerative diseases; NFT, neurofibrillary tangles; NLRP3, pyrin domain containing 3; NO, nitric oxide; NOR, novel object recognition test; NRF2, nuclear factor (erythroid-derived 2)-like 2; OS, oxidative stress; PD, Parkinson's disease; PI, propidium iodide; TFR1, transferrin receptor 1; TNF-α, tumor necrosis factor alpha; WBC, white cell counts; ZnPP, zinc protoporphyrin..

* Corresponding author. Department of Pharmacology School of Medicine-UAM Calle Arzobispo Morcillo, 4 28029, Madrid, Spain.
E-mail address: manuela.garcia@uam.es (M.G. López).

https://doi.org/10.1016/j.redox.2020.101789
Received 23 July 2020; Received in revised form 6 October 2020; Accepted 2 November 2020
Available online 6 November 2020

brain, they constitute the resident immune cells of the central nervous system (CNS) and play pivotal roles in development, plasticity and controlling neuroinflammation. Under physiological conditions, microglia are in a "surveying" state, in which they acquire a specific phenotype with a ramified morphology [10]. Upon an acute insult, they acquire an "activated" state and experience a phenotypic change into an amoeboid morphology; they produce and release different inflammatory molecules, such as cytokines (IL-1β, TNF-α) or oxidant species, as nitric oxide (NO), which may be toxic, but are also required to confront the insult [11–13]. However, with aging, microglial cells experience a shift in their phenotype to a constant activated state, known as "primed" microglia, creating a feedforward loop and promoting tissue atrophy, neurotoxicity and cognitive decline [10,14,15].

Heme oxygenase-1 (HO-1) is an inducible enzyme that catabolizes the heme group into carbon monoxide (CO) and biliverdin, which rapidly converts to bilirubin, and labile iron (Fe^{2+}). Under physiological conditions, HO-1 expression is found at very low levels in the CNS. However, the Hmox1 promoter presents different response elements that can rapidly induce its expression, mainly in glial cells in the brain, by products such as heavy metals, inflammatory mediators (TNF-α, β-amyloid) or molecules (lipopolysaccharide (LPS). A tight regulation of HO-1 is crucial as an unbalance in its activity is linked with the pathogenesis and progression of neuroinflammation, aging and NDDs [16,17]. On one hand, HO-1 induction in the brain has been reported to confer neuroprotection against OS and inflammation (LPS, β-amyloid) in models of aging, Alzheimer's disease (AD) [18–20], Parkinson's disease (PD) [21,22], experimental autoimmune encephalomyelitis (EAE) [23], subarachnoid hemorrhage [24] or brain ischemia [25]. On the other hand, systemic inflammation in the elderly can increase the expression of HO-1, but rather than having neuroprotective effects, it can cause cognitive impairment [8,9]. Furthermore, human HO-1 overexpression in astrocytes replicates parkinsonian features [26–28], and salivary upregulated levels of HO-1 have been proposed as a PD marker [29]. In addition, long-term induction of HO-1 impairs the recovery of mice subjected to intracerebral hemorrhage [30]. In AD-like mouse models, up-regulation of HO-1 causes cognitive decline and worseness tauopathy progression [31]. Therefore, induction of HO-1 has shown to provide opposed effects in aging and NDDs.

The negative outcomes reported above for HO-1 overexpression may be related to the accumulation of iron derived from HO-1 catabolism. Related to this, in aging or in situations where HO-1 is up-regulated, there is an increase in the iron content alongside with alterations of different iron-related metabolism transporters and proteins in the brain [32–37], where microglial cells play a major role [38–40]. Furthermore, these alterations are linked with cognitive impairment, protein aggregation and OS and, ultimately, to neuronal death [41,42]. In this respect, ferroptosis is a specific type of regulated cell death related to iron-dependent accumulation of lipid hydroperoxides of poly-unsaturated fatty acids (PUFA). Glutathione peroxidase 4 (GPX4) is a ferroptotic marker as it converts toxic lipid hydroperoxides to non-toxic alcohols. In iron-related toxic environments, GPX4 protein is found to be decreased, leading to the accumulation of toxic lipid hydroperoxides and cell death [43–45].

With this background in mind, this study was designed to understand the role of microglial HO-1 in aging under pro-inflammatory conditions. Our results evidence that microglial HO-1 overexpression in aged mice exposed to an acute inflammatory insult favors iron accumulation, ferroptosis and memory impairment, all conditions relevant to neurodegeneration. Therefore, strategies aimed to modulate microglial HO-1 or reduce iron accumulation could be of interest to treat age-dependent NDDs.

2. Materials and methods

2.1. Materials

Lipopolysaccharide (LPS, serotype O127:B8), deferoxamine (DFX) and propidium iodide (PI) were purchased from Sigma-Aldrich (Madrid, Spain). Zinc protoporphyrin (ZnPP) was obtained from Frontier Scientific (Madrid, Spain). 2′,7′-dichlorodihydrofluorescein diacetate probe (H_2DCFDA), dihydroethidium probe (DHE) and Hoechst were acquired from Thermo Fisher (Madrid, Spain).

2.2. Animals

All animals were housed on a 12 h light/12 h dark cycle, with food and water *ad libitum* in a conventional animal facility. All efforts were made to minimize animal suffering and to reduce the number of animals used. All experimental procedures were performed following the Guide for the Care and Use of Laboratory Animals and were previously approved by the institutional Ethics Committee of the Universidad Autónoma de Madrid and the Comunidad Autónoma of Madrid, Spain, (PROEX 252/16) following the European Guidelines for the use and care of animals for research in accordance with the European Union Directive of September 22, 2010 (2010/63/UE) and with the Spanish Royal Decree of February 1, 2013 (53/2013).

2.3. Generation of LyzMCreHMOX1 mice

Cell-specific knockout (KO) mice in HMOX1 ($LyzM_{cre}HMOX1^{f/f}$: $HMOX1^{M\text{-}KO}$) were generated using the cre/LoxP system at the Universidad Autónoma de Madrid. For that purpose, $LyzM_{cre}$ (The Jackson Laboratory: B6.129P2-Lyz2tm1(cre)Ifo/J, stock.: 004781) mice, which carry the *cre* recombinase under the control of a myeloid promoter; and $HMOX1_{LoxP}$ (RIKEN BioResource Center, stock.: RBRC03163) mice were crossed resulting in a heterozygous offspring for both the *cre* recombinase and the *LoxP* site. The heterozygous mice were crossed and the homozygous offspring for the *LoxP* site carrying the *cre* recombinase were used for the experiments ($HMOX1^{M\text{-}KO}$). In these mice, the *cre* recombinase mediates a specific deletion of *LoxP*-flanked HMOX1 gene in myeloid cells, therefore in microglial cells in the brain. Adult (3-4 months-old) and aged mice (15-18 months-old) were used for these experiments. Age-matched littermates (WT), which are mice carrying the *LoxP* sites but not the *cre* recombinase were used as controls.

The polymerase chain reaction (PCR) was used to genotype mice (Fig. S1) using genomic DNA from ear notches and the following primers: *LoxP* site (5′-3′): 1) Forward Hmox1 wild type: CTC ACT ATG CAA CTC TGT TGG AGG, 2) Reverse Hmox1 wild type: GTC TGT AAT CCT AGC ACT CGA A, 3) Reverse Hmox1 *LoxP*: GGA AGG ACA GCT TCT TGT AGT CG. $LyzM_{cre}$ allele (5′-3′): 1) Mutant: CCA GAA ATG CCA GAT TAC G, 2) Common: CTT GGG CTG CCA GAA TTT CTC, 3) Wild type: TTA CAG TCG GCC AGG CTG AC. As shown in Fig. S1, in the presence of the recombinase, HO-1 is only depleted in microglial cells in the brain [24].

2.4. LPS in vivo model

Aged (15–18 months) $HMOX1^{M\text{-}KO}$ and WT male mice were intraperitoneally injected (i.p.) with 0.5 mg/kg of LPS or saline. Weight and sickness-related behavioral tests were recorded before the LPS treatment and 4, 8 and 24 (final point) hours after the injection. At the final point, mice were sacrificed and the brain collected for further analysis.

2.5. Pharmacological treatments

Inhibition of HO-1 was achieved using Zinc Protoporphyrin (ZnPP). For that purpose, 2 h before the LPS injection, ZnPP at 25 mg/kg was administered i.p. to aged WT mice. ZnPP was prepared just before the

injection and dissolved in saline with 5% DMSO.

Deferoxamine (DFX) at 100 mg/kg was dissolved in saline and administered i.p. once a day for 6 consecutive days before the LPS injection. The last dose of DFX was given on the same day of the LPS treatment.

2.6. Sickness behavioral tests: locomotor activity and social interaction

-*Locomotor activity.* Animals were maintained in their home cages with a size of 26 cm × 20 cm and were videotaped during 5 min. For analysis, cages were virtually divided into 8 identical squares and the number of crossings was analyzed during the last 3 min. Results were normalized with respect to the number of crossings of the same animal before the LPS injection, which was considered as 100%.

- *Social interaction.* Social exploratory behavior was determined as a measure of sickness behavior, as previously described [46]. For these experiments, a juvenile novel mouse (4 weeks of age) was introduced in the cage during 10 min and the exploratory activity was videotaped. The total amount of time that the experimental mice was engaged in social investigation of the juvenile (e.g., anogenital sniffing, trailing) was monitored. Results were normalized with those obtained for the same animal at basal conditions before LPS injection, which was considered as 100%.

2.7. Cognitive behavioral test: novel object recognition test (NOR)

The novel object recognition test (NOR), was used to assess the cognitive status (recognition memory) of the experimental mice and was performed as previously described [47]. This test is divided into 3 consecutive days (Fig. 3**G**); on the first day (T0), the experimental mice are placed in a 40 cm × 40 cm x 40 cm cage for 10 min. The next day (T1), the mice are placed in the same cage but with two identical objects in shape and color. The test itself (T2) is performed 48 h after the habituation test. In order to asses if the animals have cognitive decline, one of the objects is changed for a different one, both in shape and color. The amount of time spent exploring the novel (TN) or familiar (TF) object was recorded and the differences were represented as Discrimination Index (DI). Mice have an innate preference for novelty, thus mice without cognitive impairment will recognize the familiar object and will spend most of the time at the novel object. DI allows discrimination between the novel and familiar objects and it is calculated as follows DI = (TN-TF)/(TN + TF). For this test, the LPS administration was given just after T1 (second day).

2.8. Oxidative stress and cell death measurements

After a given treatment, HMOX1$^{M\text{-}KO}$ and WT mice were sacrificed,

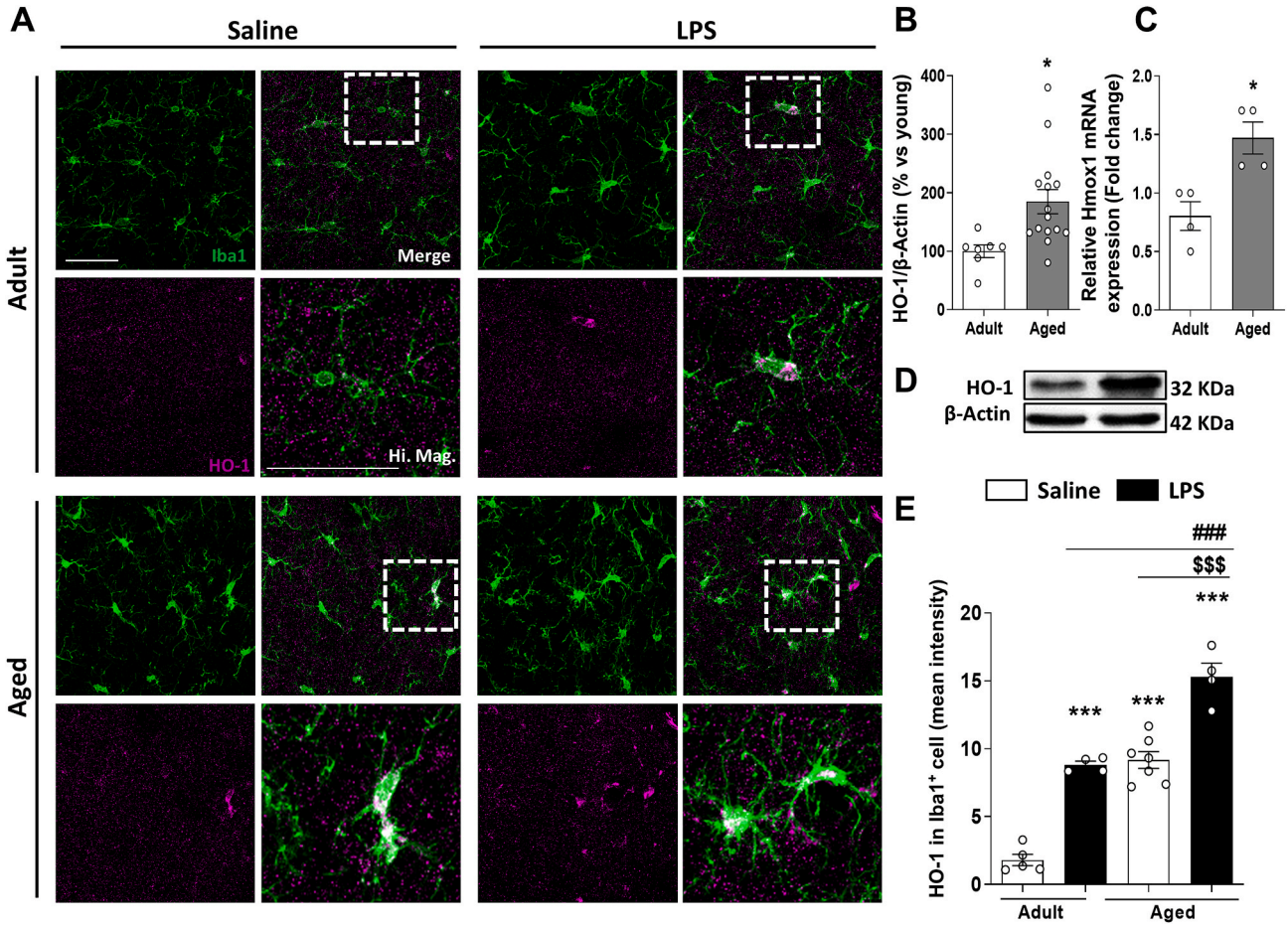

Fig. 1. Microglial HO-1 is overexpressed in aged *vs* adult mice and when peripherally stimulated with LPS. (**A**) Representative images for Iba1+ microglia (green) and HO-1 (magenta) in adult and aged mice. Quantification (**B**) and representative blot images (**D**) of HO-1 protein expression and mRNA levels (**C**) in brain. HO-1 is found overexpressed in aged mice in comparison to adult mice. As shown in the quantification of HO-1 expression in Iba1+ microglial cells, measured as mean intensity (**E**), microglial HO-1 is found overexpressed in aged mice injected with LPS in comparison to aged mice treated with saline and adult mice treated with or without LPS. Data represent mean ± S.E.M. (N = 4–15, Student's *t*-test (**B**, **C**) and one-way ANOVA followed by Tukey's post-hoc test (**E**). Significant differences were considered when: *p < 0.05 and ***p < 0.001 compared to adult WT mice treated with saline; ###p < 0.001 in comparison to adult mice stimulated with LPS and $$$p < 0.001 in comparison to aged mice treated with saline. Scale bar = 9 μm. (For interpretation of the references to color in this figure legend, the reader is referred to the Web version of this article.)

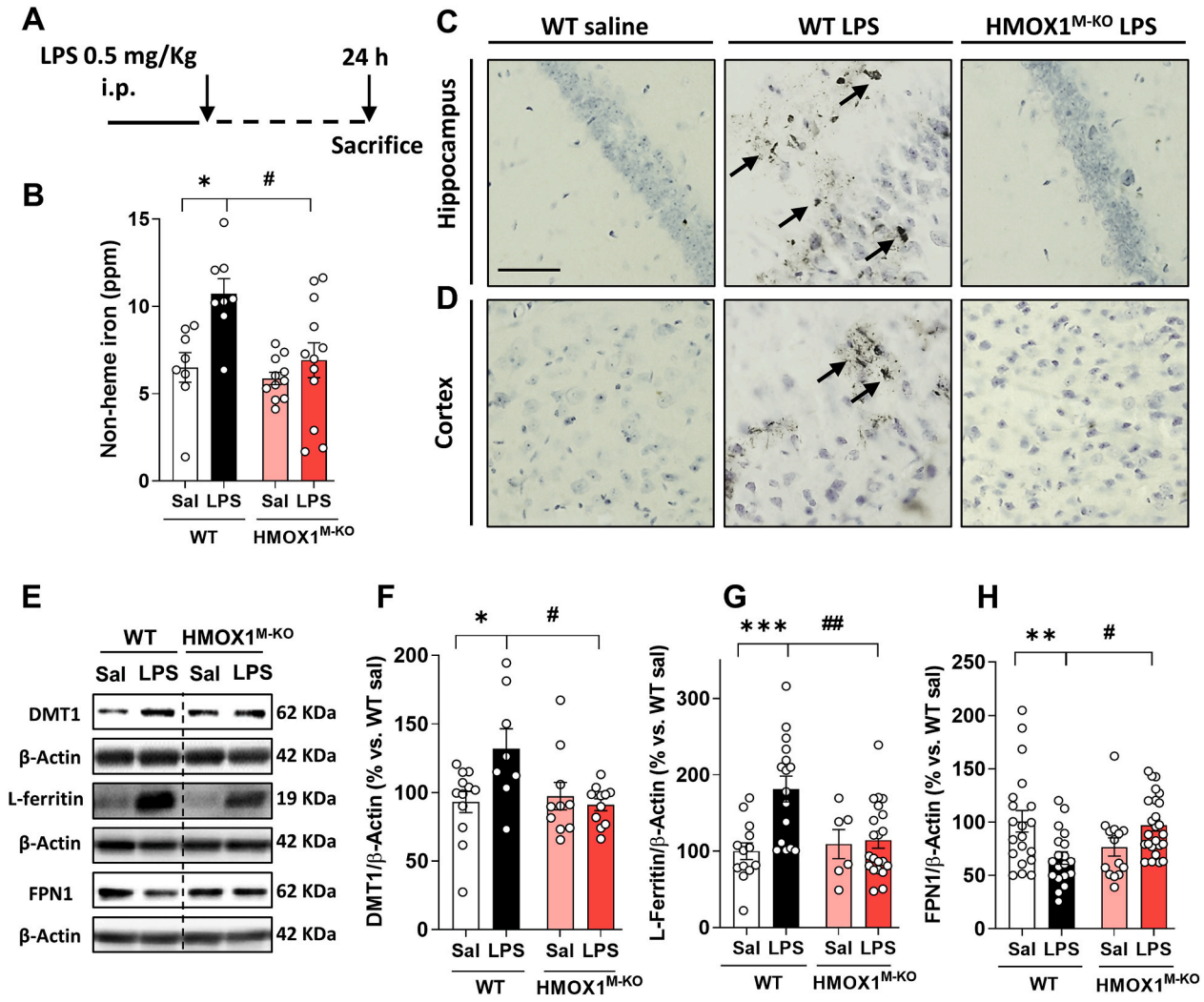

Fig. 2. LPS leads to iron accumulation and alterations in iron metabolism markers in aged WT mice, but not in microglial HO-1 knock-out mice. (**A**) Scheme of the experimental protocol. LPS increases non-heme iron accumulation in the brain of aged WT mice (**B**), and increases iron deposits as Perl's solution representative images show in hippocampus (**C**) and cortex (**D**) in comparison to WT saline mice. These alterations were restored in HMOX1^{M-KO} mice challenged with LPS. (**E**) LPS led to alterations in different iron metabolism markers in the hippocampus of WT mice. LPS increased DMT1 (**F**), and L-ferritin protein levels (**G**). Moreover, the levels of ferroportin (FPN1) were significantly reduced in aged WT mice injected with LPS (**H**). These alterations were partially restored in the brain of aged HMOX1M-KO mice. Data represent mean ± S.E.M. (N = 6–22, one-way ANOVA followed by Tukey post-hoc test). Significant differences were considered when: *p < 0.05, **p < 0.01 and ***p < 0.001 compared to aged WT saline mice or #p < 0.05 and ##p < 0.01 compared to aged WT LPS injected mice. Arrows indicate ferric iron accumulation. Scale bar = 50 μm.

the hippocampi dissected in ice-cold Krebs's dissection buffer (120 mM NaCl; 2 mM KCl; 26 mM $NaHCO_3$; 1.18 mM KH_2PO_4; 10 mM $MgSO_4$; 0.5 mM $CaCl_2$; 11 mM glucose and 200 mM sucrose at pH 7.4) and cut into 250 μm thick slices to measure OS and cell death. The slices were stabilized in pre-incubation solution (120 mM NaCl; 2 mM KCl; 26 mM $NaHCO_3$; 1.18 mM KH_2PO_4; 10 mM $MgSO_4$; 0.5 mM $CaCl_2$ and 11 mM glucose) and oxygenated for 45 min in a water bath at 34 °C. Thereafter, hippocampi slices were incubated in control solution (120 mM NaCl; 2 mM KCl; 26 mM $NaHCO_3$; 1.18 mM KH_2PO_4; 10 mM $MgSO_4$; 2 mM $CaCl_2$ and 11 mM glucose) at 37 °C for 40 min with the fluorescent dye propidium iodide (PI: 1 μg/mL) to measure cell death and H_2DCFDA (10 μM) and DHE (2,3 μM) to determine OS. Fluorescence was measured with an inverted Nikon eclipse T2000-U microscope (Nikon Instruments) under a 2X objective. Wavelengths of excitation and emission for PI, H_2DCFDA and DHE were 530, 495, 500 and 580, 520, 600, respectively. The mean intensity was analyzed with Fiji software.

2.9. RNA extraction and Real Time quantitative polymerase chain reaction (RT-qPCR)

Total RNA was extracted using Trizol reagent (Sigma-Aldrich, Spain) and quantified using a Nanodrop Spectrophotometer (Nanodrop 2000, Thermo Scientific). 1 μg of RNA was reversely transcribed using PrimeScript RT Reagent Kit (perfect Real Time) (Takara, Japan) and the quantitative RT-qPCR was performed using qPCRBIO SyGreen Mix Lo-Rox polymerase (Cultek) and a 7500 Fast Real-Time PCR System (Applied Biosystems by Life Technologies). Thermal cycling for RT-qPCR was carried out according to the manufacturer's recommendations, and the relative expression levels were calculated using the comparative ΔΔCt method. The primer's sequences (5' – 3') were as follows (from Sigma-Aldrich, Madrid, Spain): β2-microglobulin as house-keeping gene (FWD: ACC GTG ATC TTT CTG GTG CTT G; RVS: TAG CAG TTG AGG AAG TTG GGC T), IL-1β (FWD: GAA GAG CCC ATC CTC TGT GA; RVS: TTC ATC TCG GAG CCT GTA GTG) and TNF-α (FWD: CAT CTT CTC AAA ATT CGA GTG ACA A; RVS: TGG GAG TAG ACA AGG TAC AAC CC).

2.10. Western blot (WB)

Hippocampi from mice were lysed in ice-cold AKT lysis buffer (137 mM NaCl, 20 mM NaF, 10% glycerol, 20 mM Tris–HCl, 1% Nonidet P-40, 1 μg/mL leupeptin, 1 mM phenylmethylsulfonylfluoride, 1 mM sodium pyrophosphate, and 1 mM Na_3VO_4, pH 7.5). Protein quantification was performed using the Pierce BCA Protein Assay Kit (ThermoFisher) and 10 μg of protein was resolved by sodium dodecyl sulfate-polyacrylamide (SDS-PAGE) gel and transferred to Immobilon-P PVDF membranes (Millipore Corp.). For the antibody incubation, membranes were activated with methanol and blocked with 4% bovine serum albumin (BSA) in Tris-buffered saline-Tween (TTBS: 10 mM Tris, 150 mM NaCl; 0.2% Tween-20, pH 7.4) for 2 h. Afterwards, membranes were incubated overnight at 4 °C with the primary antibodies: anti-iNOS (1:1000, 610432, BD Transduction Laboratories), anti-p65 (1:1000, sc-372, Santa Cruz Biotechnology), anti–HO–1 (1:1000, ab68477, Abcam), anti-DMT1 (1:1000, sc-166884, Santa Cruz Biotechnology), anti-L-ferritin (1:500, sc-390558, Santa Cruz Biotechnology), anti-CD68 (1:500, MCA1957GA, Bio-Rad Laboratories), anti-FPN1 (1:1000, NBP1-21502, Novus Biologicals), anti-GPX4 (1:1000, ab125066, Abcam), anti-Caspase-1 (1:1000, AG-20B-0042-C100, AdipoGen Life Science), anti-NLRP3 (1:1000, AG-20B-0014-C100, Adipogen Life Science), anti-IL-1β (1:50, sc-12742, Santa Cruz Biotechnology), anti-β-actin (1:50000, A3854, Sigma-Aldrich). Thereafter, the membranes were washed with TTBS and incubated for 2 h with the appropriate peroxidase-conjugated secondary antibodies (1:10 000, Santa Cruz Biotechnology). Membranes were washed and then incubated with ECL Advance Western-blotting Detection Kit (GE Healthcare, Amersham). Finally, they were exposed using the ChemiDoc MP System (Bio-Rad Laboratories) and the specific bands were analyzed with Fiji software.

2.11. Tissue immunofluorescence

Mice were deeply anesthetized by an intraperitoneal injection of sodium pentobarbital, perfused with saline and fixed with 4% paraformaldehyde (PFA). Brains were removed and kept overnight at 4 °C in 4% PFA. Then, the tissue was cryoprotected for 2 days in 30% sucrose and 40 μm thick coronal slices were cut using a sliding microtome and collected in phosphate buffer (PB) 0.1 M. For the immunofluorescence assay, sections were blocked with 5% goat or donkey serum for 2 h. Afterwards, sections were incubated at 4 °C with the primary antibodies: anti-Iba1 (1:400, two days incubation, ab5076, Abcam), anti–HO–1 (1:500, overnight, Abcam), anti-GPX4 (1:500, overnight, Abcam) or anti-CD68 (1:500, overnight, Bio-Rad Laboratories). Sections were washed three times and then incubated with the secondary fluorescent antibody (1:200, Alexa Fluor 488 or 546, ThermoFisher) for 1 h. After three washes, sections and cells were mounted and the images taken in a SP-5 confocal microscope (TCS SPE; Leica). Image analysis was performed using Fiji software.

2.12. Perl's solution

Brain sections (40 μm) were washed for 30 min in PB 0.1 M and then incubated in Perl's solution (5% potassium ferrocyanide: 5% HCl, 1:1, v:v) for another 30 min at room temperature (RT). Sections were washed with PB 0.1 M for 30 min and then incubated in diaminobenzidine (DAB, 0.05% DAB in PB 0.1 M) for 20 min. In order to start the reaction, sections were exposed to hydrogen peroxide (0.003% in PB 0.1 M) for 20 min. Then, to stop the reaction, sections were washed three times with PB 0.1 M. Sections were mounted in 1:3 diluted PB 0.1 M and dried overnight at RT. Afterwards, sections were briefly washed in water and counterstained for 15 s with 0.1% Cressyl Violet at RT. Sections were washed in distilled water, dehydrated following a gradient of alcohols and degreased in xylene for 30 min and, finally, covered with Depex. Sections were examined and photographed under transmitted light microscopy in an OlympusBX61 microscope using an oil-immersion 40x objective, and a DP71 video-camera (Olympus-Europa, Hamburg, Germany).

2.13. Non-heme iron determination

Brain samples were weighted before the procedure and then incubated with 2 mL of 10% trichloroacetic acid and 3 M HCl (acid solution) for 20 h at 65 °C. Samples (80 μL) were mixed with the reaction buffer (10% thioglycolic acid in 1 M sodium acetate solution) followed by a mixture of the colorimetric solution (1% bathophenanthroline disulfonic acid) in a 1:1 vol ratio. To quantify the non-heme iron content, a calibration curve was performed using serial dilutions of an iron standard solution (VWR) presented in ppm (parts per million: μg of non-heme iron per grams of wet tissue). Optical density was measured at 535 nm in a microplate reader (SPECTROstar NANO, BMG Labtech).

2.14. Statistics

Data are represented as the mean ± S.E.M and were analyzed using GraphPad Prism 8.02 version software. Two-groups were compared with the Student's *t*-test, while multiple groups were compared using one-way analysis of variance test (ANOVA followed by the Tukey post hoc test). Data from sickness behavioral tests with repetitive measurements on individual animals (different time points) were analyzed using two-way ANOVA (followed by the Tukey post-hoc test). Statistical significance was set at $*p < 0.05$, $**p < 0.01$ and $***p < 0.001$. Statistical trends were considered when $p < 0.10$.

3. Results

3.1. HO-1 is up-regulated in microglial cells in the brain of mice stimulated with LPS and in aging

HO-1 is a well-known anti-oxidant and anti-inflammatory enzyme, thus its induction has been proposed as a therapeutic target for the treatment of different neuroinflammatory and aged-related NDDs. However, there is still controversy on whether HO-1 is down or up-regulated in these diseases [16,17,20,48–50]. In this study, HO-1 was found up-regulated in the brain of aged mice in comparison to adult mice (Fig. 1A–D). This agrees with our recent finding where HO-1 overexpression with aging occurred mainly in the microglial compartment in comparison to other cell types from the CNS [51].

Inflammation is one of the main pathological hallmarks in aging and other related NDDs, where microglial HO-1 is found up-regulated. Therefore, we aimed to study the impact of an acute inflammatory insult in HO-1 expression under these circumstances. The levels of this enzyme in Iba1+ microglial cells was significantly induced in aged mice treated with LPS in comparison to age-matched controls, treated with both saline or LPS (Fig. 1A and E). These results indicate that with aging microglial HO-1 is upregulated and its overexpression is further increased under an acute inflammatory insult. In order to further understand the role of microglial HO-1 up-regulation in our model, and whether it could be acting as a mechanism of compensation or creating a feedforward loop favoring disease progression, we have generated a cell specific knock-out mouse ($HMOX1^{M\text{-}KO}$), which lacks HO-1 in the myeloid cells, and therefore in microglia (Fig. S1). These mice are born at Mendelian ratios, develop normally, do not develop microcytic anemia (Table S1), exhibit normal white cell counts (WBC) (Fig. S2) and have a life span similar to that of WT mice [52,53].

3.2. Depletion of microglial HO-1 in aged mice restores the iron metabolism alterations observed under an inflammatory environment

In spite of the anti-oxidant and anti-inflammatory properties described for HO-1, the catabolism of the heme group by this enzyme also generates labile iron, which can accumulate leading to cytotoxic

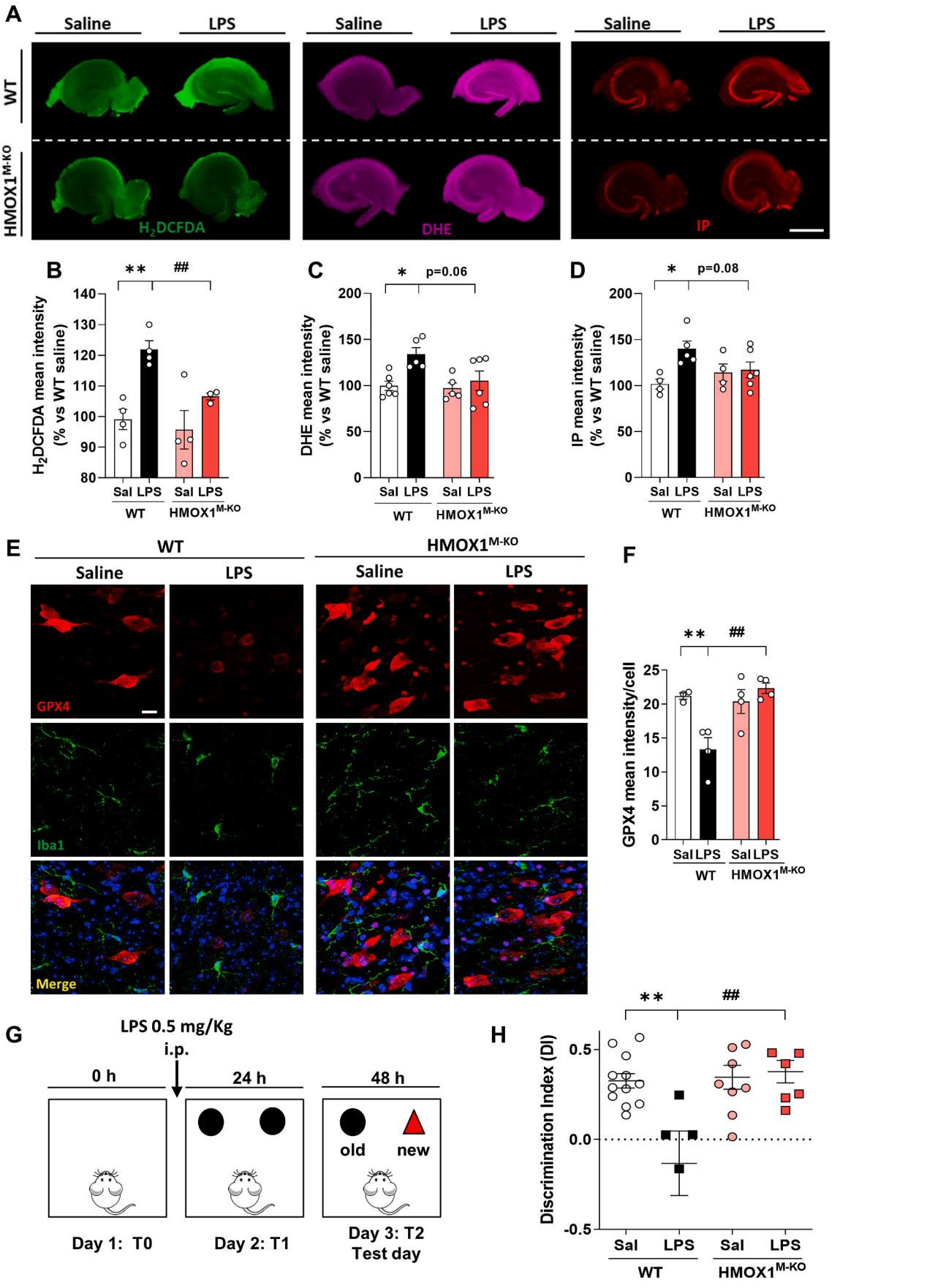

(caption on next page)

Fig. 3. Aged WT mice treated with LPS showed increased oxidative stress, ferroptosis and cognitive decline, but these alterations were prevented in HMOX1$^{M\text{-}KO}$ mice. (**A**) Representative images in whole hippocampal slices of reactive oxygen species (ROS) measured with the fluorescent probes H_2DCFDA, dihydroethidium (DHE) and hippocampal cell death, measured with the fluorescent dye propidium iodide (IP). (**B**) Quantification of H_2DCFDA mean intensity, (**C**) DHE mean intensity and (**D**) propidium iodide mean intensity in whole hippocampal slices. Representative images (**E**) and quantification (**F**) of GPX4 (red), a ferroptotic marker. (**G**) Schematic representation of the novel objet recognition test (NOR). LPS (0.5 mg/kg) was injected just before day 2 (T1) and 24 h after, the test (T2) was performed. (**H**) Discrimination index (DI) in control and LPS treated mice. WT mice treated with LPS showed an increase in cognitive decline, measured as a reduction in the DI, which was restored in HMOX1$^{M\text{-}KO}$ mice treated with LPS. Data represent mean ± S.E.M. (N = 3–12, one-way ANOVA followed by Tukey post-hoc test). Significant differences were considered when: *p < 0.05 and **p < 0.01 compared to aged WT saline mice or ##p < 0.01 compared to aged WT LPS injected mice. Scale bar = 1000 μm (**A**) and 10 μm (**E**). (For interpretation of the references to color in this figure legend, the reader is referred to the Web version of this article.)

effects when HO-1 is overexpressed [41,42]. Therefore, we aimed to study the consequences of microglial HO-1 overexpression and its depletion during aging in an inflammatory *in vivo* model. For that purpose, WT and HMOX1$^{M\text{-}KO}$ aged mice were treated with saline or LPS (0.5 mg/kg i.p.) for 24 h (Fig. 2A). Firstly, we wanted to know if the up-regulation of HO-1 induced by LPS led to an increase in iron deposits in the brain. A significant increase in non-heme iron was found in the brain of aged WT mice injected with LPS, but this increase was not observed in the HMOX1$^{M\text{-}KO}$ mice challenged with LPS (Fig. 2B). Furthermore, Perl's solution staining indicated that iron was accumulating in LPS injected WT mice in hippocampus and cortex (Fig. 2C and D) and also in thalamus and amygdala (figs. S3A and B) in comparison to WT saline mice. Interestingly, these deposits were lower in HMOX1$^{M\text{-}KO}$ mice treated with LPS (Fig. 2C and D), thus suggesting that LPS-dependent microglial HO-1 up-regulation in aging could play a pivotal role in the formation of iron deposits.

The iron deposits observed in the brain of WT mice treated with LPS were linked to alterations in different iron metabolism markers (Fig. 2E). While there was an increase in the iron importer DMT1 (Fig. 2E and F) and in the storage protein L-ferritin (Fn) (Fig. 2E and G), there was a decrease in the iron exporter protein FPN1 (Fig. 2E and H). However, these alterations were reverted in HMOX1$^{M\text{-}KO}$ mice treated with LPS, meaning that in aged WT mice, LPS caused a higher iron influx and storage and a lower efflux in cells leading to iron accumulation. Of note is that in aged HMOX1$^{M\text{-}KO}$, the previous alterations in the iron flux within the cells were not observed, suggesting that iron was not accumulating.

3.3. An inflammatory stimulus causes brain oxidative stress, ferroptosis and cognitive decline in aged WT mice, but not in aged HO-1 microglial knock-out mice

Iron overload generates oxidative stress through the *Fenton reaction* leading to a specific type of cell death, known as ferroptosis [43–45]. To elucidate whether iron accumulation mediated by LPS-induced microglial HO-1 overexpression could be causing OS, cell death, and ferroptosis, different markers were evaluated. The fluorescent dyes H_2DCFDA (Fig. 3A and B) and DHE (Fig. 3A and C) were used to assess ROS production in the hippocampi of WT and HMOX1$^{M\text{-}KO}$ mice treated with saline or LPS. Both markers were significantly increased in aged WT mice in comparison to WT saline mice (Fig. 3B and C). However, in HMOX1$^{M\text{-}KO}$ mice challenged with LPS, there was a significant decrease in ROS production, represented as a significant reduction in H_2DCFDA intensity and a statistical trend ($p = 0.06$) in DHE fluorescence. Moreover, LPS injection in WT mice led to an increase in hippocampal cell death, measured by PI dye. However, HMOX1$^{M\text{-}KO}$ mice treated with LPS showed a tendency to reduction in cell death (Fig. 3A and D). Furthermore, to specifically evaluate ferroptosis, glutathione peroxidase 4 (GPX4) was analyzed. This antioxidant enzyme catalyzes the reduction of hydrogen peroxide and lipid peroxides to protect the cells against OS. Therefore, a decrease in this marker is indicative of ferroptosis. LPS decreased the expression of GPX4 in WT mice, but not in HMOX1$^{M\text{-}KO}$ (Fig. 3E and F). As ferroptosis leads to neuronal death, we aimed to study if LPS could also result in cognitive decline, assessed with the NOR task, which is a measurement of recognition memory (Fig. 3G). Indeed, LPS induced cognitive decline in WT mice, measured as a decrease in the DI, but not in HMOX1$^{M\text{-}KO}$, which performed similar to WT mice treated with saline (Fig. 3H). Therefore, these results indicate that iron accumulation observed in aged WT mice, possibly via LPS-induced upregulation of microglial HO-1, could be responsible for OS, ferroptosis and, ultimately, cognitive decline as in HMOX1$^{M\text{-}KO}$ mice treated with LPS all these hallmarks were significantly attenuated and partially restored.

3.4. Microglial HO-1 depletion improves LPS-induced inflammatory profile and sickness behavior in aged mice

A tight regulation between iron deposits and neuroinflammation has been reported [36,54]. Therefore, we aimed to study whether LPS-dependent microglial HO-1 overexpression, apart from leading to iron metabolism alterations, could be related to pro-inflammatory changes in the brain, in spite of its anti-inflammatory properties. For that purpose, different inflammatory markers were analyzed in the hippocampus 24 h after LPS injection (Fig. 4A). In this context, proinflammatory proteins such as inducible nitric oxide synthase (iNOS) and p65 (Fig. 4B and C), alongside to inflammasome-related proteins: NLR Family Pyrin Domain Containing 3 (NLRP3), caspase-1 and interleukin 1 beta (IL-1β) (Fig. 4B and D) were measured, in addition to different cytokines such as tumor necrosis factor alpha (TNF-α) and IL-1β (Fig. 4E). WT mice injected with LPS showed a significant increase in the expression of these proteins or cytokines in comparison to WT saline mice. However, HMOX1$^{M\text{-}KO}$ mice challenged with LPS presented a significant decrease of these parameters. Moreover, all these pro-inflammatory changes in WT mice treated with LPS were accompanied by behavioral alterations, measured by the LPS-related sickness behavior [12] social interaction (Fig. 4F) and locomotion (Fig. 4G) tests, which were performed at 4, 8 and 24 h after LPS injection. Interestingly, whereas HMOX1$^{M\text{-}KO}$ mice injected with LPS showed a partial recovery 24 h after the treatment, WT mice were not able to recover and performed significantly worse than HMOX1$^{M\text{-}KO}$ mice (Fig. 4F and G). The improvements observed at the behavioral and biochemical levels in LPS treated HMOX1$^{M\text{-}KO}$ mice were accompanied by an improvement in survival (statistical trend) and with a significant lower reduction in weight loss 24 h after LPS injection (figs. S4A and B). Therefore, LPS-related labile iron brain accumulation was accompanied by an increase in inflammatory markers in the hippocampus and sickness behavior, which were greatly prevented in aged HMOX1$^{M\text{-}KO}$ mice.

3.5. LPS induced higher levels of CD68 immunoreactivity in Iba1+ microglial cells in aged WT mice, but not in HMOX1$^{M\text{-}KO}$

Our next step was to study if the inflammatory alterations previously described were accompanied by changes in the microglial phenotypic and activated profile. For this purpose, we analyzed CD68, a transmembrane glycoprotein located in the lysosomal compartment, used to specifically identify activated microglia in the brain [55]. Compared to WT saline treated mice, WT LPS injected mice showed increased hippocampal CD68 expression (Fig. 5A) and also increased levels of microglial CD68, measured as CD68 mean intensity per microglial cell (Iba1+) (Fig. 5B and C). However, these increases were not observed in HMOX1$^{M\text{-}KO}$ mice challenged with LPS. To further characterize

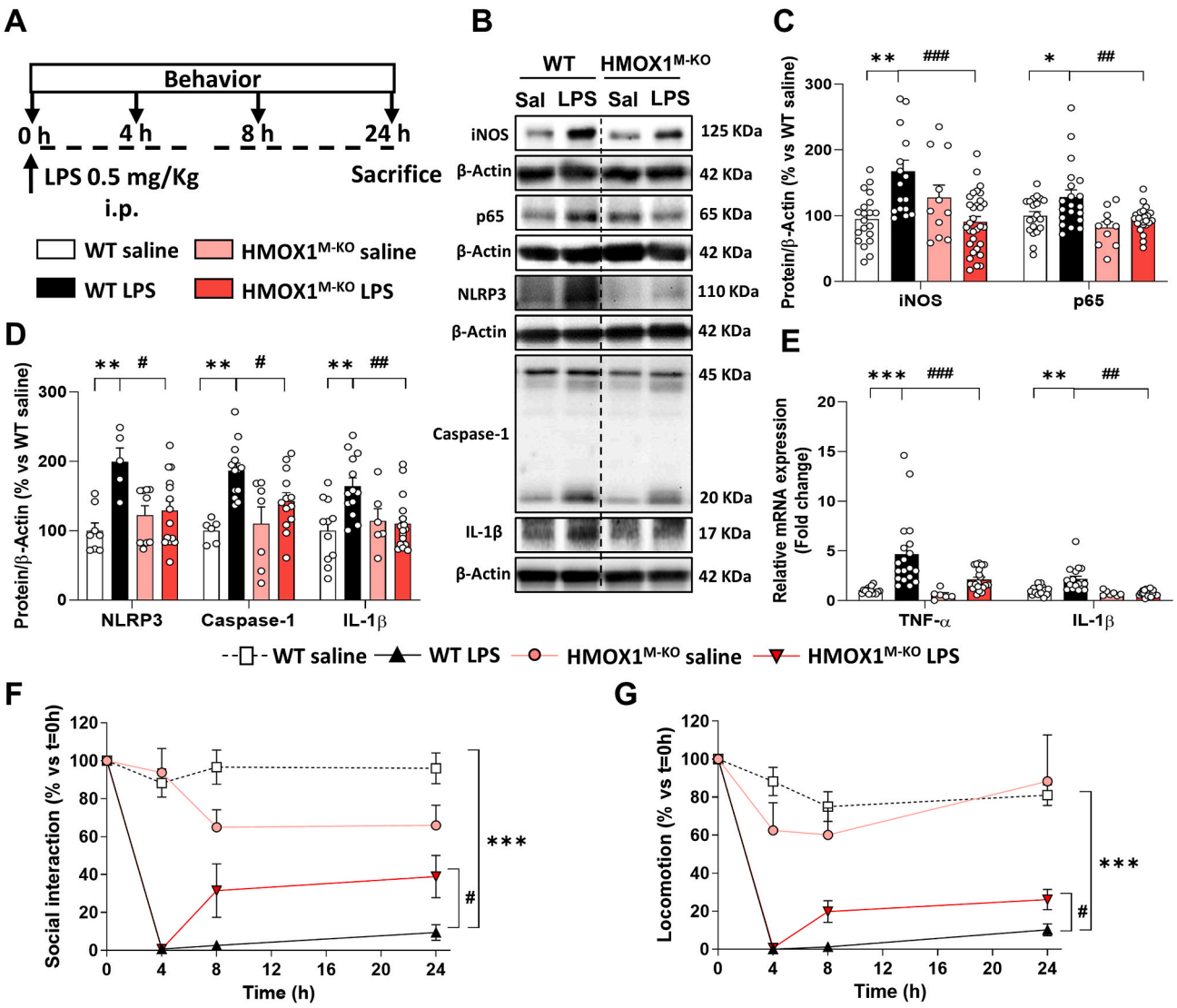

Fig. 4. Genetic depletion of microglial HO-1 improves brain inflammatory markers and LPS-induced sickness behavior in aged mice. (**A**) Scheme of the experimental protocol. LPS (0.5 mg/kg) was injected i.p. on day 0 and sickness behavioral tests were performed 4, 8 and 24 h after its administration. As shown in the representative densitometries (**B**), LPS injection in WT mice led to a significant increase in hippocampal iNOS and p65 (**C**) and in inflammasome-related proteins, such as NLRP3, caspase-1 and mature IL-1β (**D**). Moreover, LPS induced the upregulation of the pro-inflammatory cytokines TNF-α and IL-1β (**E**). Interestingly, none of the above-mentioned inflammatory alterations were observed in HMOX1$^{M\text{-}KO}$ mice challenged with LPS. LPS-related inflammatory changes led to sickness behavior, measured as social interaction (**F**) and locomotion (number of crossings) (**G**). These functional alterations were significantly restored in HMOX1$^{M\text{-}KO}$ mice. Data represent mean ± S.E.M. (N = 5–25, one-way ANOVA followed by Tukey post-hoc test). Significant differences were considered when: *p < 0.05, **p < 0.01 and ***p < 0.001 compared to aged WT saline mice or #p < 0.05, ##p < 0.01 and ###p < 0.001 compared to aged WT LPS injected mice (**C-E**). Data represent mean ± S.E.M. (N = 4–10, two-way ANOVA followed by Tukey post-hoc test). Significant differences were considered when: ***p < 0.001 compared to aged WT saline mice or #p < 0.05 compared to aged WT LPS injected mice (**F-G**).

microglial phenotypic profile, we performed another analysis focusing on CD68 occupancy within Iba1+ microglia as well as microglial morphology [55]. Thus, CD68 levels were evaluated on a scale ranging from 0 (low CD68 occupancy) to 3 (high CD68 occupancy), where the higher the given score, the higher the microglial activation (Fig. 5D). As shown in Fig. 5E, in WT mice treated with LPS there was a significant decrease in *score 1* and an increase in *score 2* and *3*, suggesting a higher activated state of microglia in comparison to WT saline mice. However, in HMOX1$^{M\text{-}KO}$ mice treated with LPS, the percentage of total microglial cells with *score 3* was significantly lower than in WT mice, and showed an increase in *score 1*, thus implying that microglia from HMOX1$^{M\text{-}KO}$ mice presented a less activated state than those from WT mice. Furthermore, morphological microglial analysis (Fig. 5F), represented with a scale, ranking from 0 (more ramified phenotype) to 3 (more amoeboid phenotype) was performed. The activated state induced by LPS in the WT mice, represented as a significantly increase in *score 3* and a decrease in *score 1*, was reverted in HMOX1$^{M\text{-}KO}$ mice (Fig. 5G). These results reinforce that microglial HO-1 depletion under an inflammatory stimulus is linked to a less activated microglia in aged mice.

3.6. *Pharmacological inhibition of HO-1 with zinc protoporphyrin (ZnPP) restores the inflammatory, oxidative and iron alterations induced by LPS*

To corroborate the results obtained with the genetic mouse model, we also performed a pharmacological approximation. For that purpose, ZnPP was used as a HO-1 inhibitor, following the protocol in Fig. 6A. ZnPP reduced non-heme iron accumulation induced by LPS (Fig. 6B), and as shown in the representative blot images (Fig. 6C) it was able to restore, at least partially, the LPS-induced iron metabolism alterations (Fig. 6D). In addition, ZnPP treatment decreased the LPS-induced

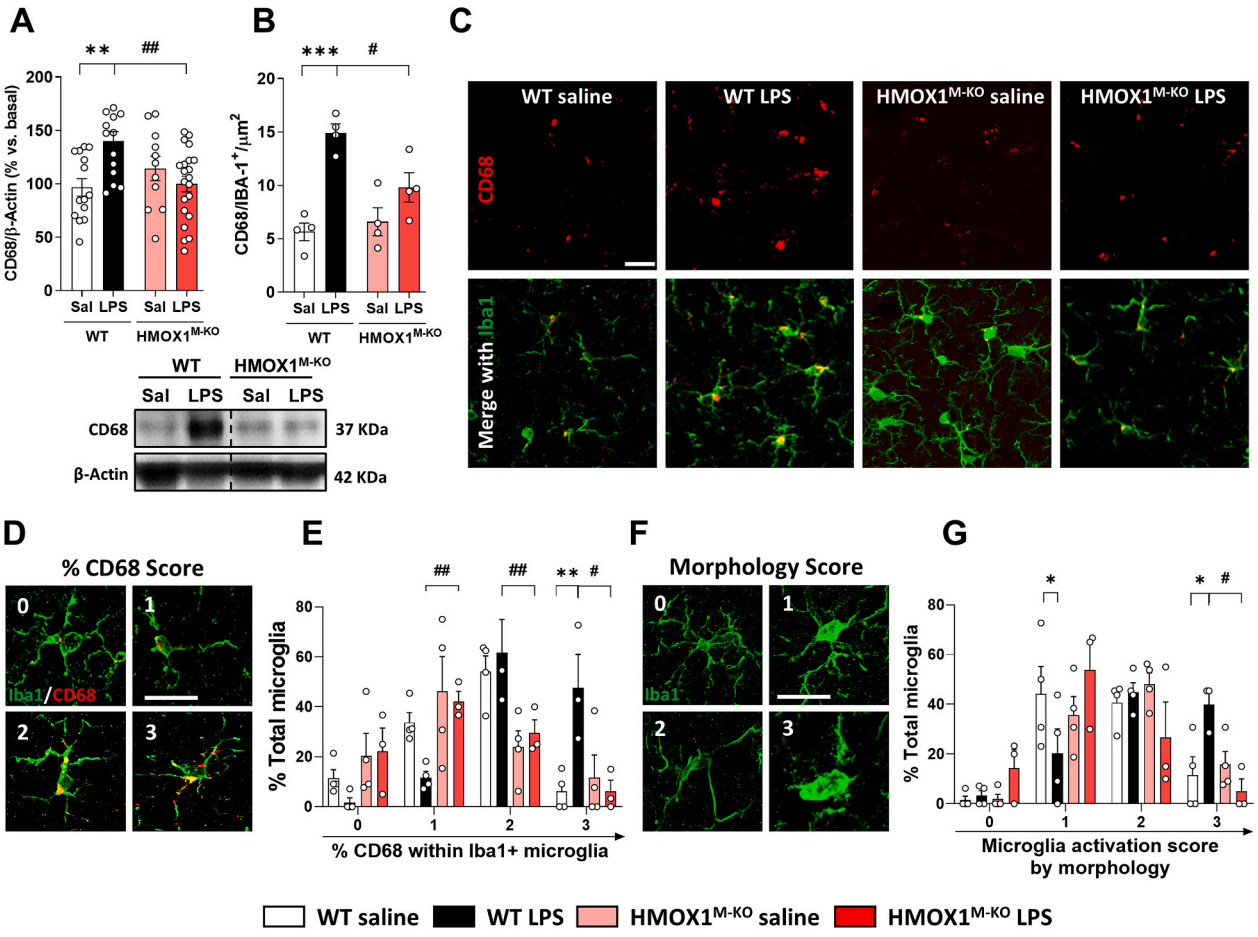

Fig. 5. Microglial activated phenotype was increased in aged WT mice treated with LPS, but not in microglial HO-1 knock-out mice. (**A**) Representative densitometry and quantification showing the increase in CD68 expression led by LPS injection in the hippocampus of aged WT mice. (**B**) Quantification and representative hippocampal immunofluorescences of CD68 (red) and Iba1+ microglia (green) (**C**). CD68 protein levels were restored to saline levels in aged HMOX1^{M-KO} mice injected with LPS. (**D**) Representative images of the scoring of CD68 occupancy within Iba1+ cells and its quantification (**E**). (**F**) Represents the morphology scores used to quantify microglia activation and its quantification (**G**). Data represent mean ± S.E.M. (N = 4–21 (**A**) and N = 3–4 (**B, E** and **G**), one-way ANOVA followed by Tukey post-hoc test). Significant differences were considered when: *p < 0.05 and **p < 0.01 and ***p < 0.001 compared to aged WT saline mice or #p < 0.05 and ##p < 0.01 compared to aged WT LPS injected mice. Scale bar = 25 μm (**C**) and scale bar = 13 μm for high magnification images (**D** and **F**). . (For interpretation of the references to color in this figure legend, the reader is referred to the Web version of this article.)

increase of iNOS, p65 and CD68 (Fig. 6E and F), the expression of the inflammasome-related proteins, mature IL-1β, NLRP3 and caspase-1 (Fig. 6G and H) and the cytokines TNF-α and IL-1β (Fig. 6I). Moreover, ZnPP improved mice performance in the sickness behavioral tasks (Fig. 6J and K) and was able to decrease mice weight loss (Fig. S4C). Taken together, these results support the role of HO-1 in the alterations related to iron metabolism, inflammation and behavior in aged mice challenged with an inflammatory stimulus.

3.7. Deferoxamine treatment improves iron metabolism alterations, inflammation and sickness behavior in aged mice treated with LPS

We have shown that microglial HO-1 increases with age and, under these conditions, a proinflammatory stimulus (LPS) results in an even higher up-regulation of this enzyme, leading to iron accumulation, brain inflammation, OS, cell death and cognitive decline. To corroborate that iron accumulation is linked to the pathological changes observed in WT mice subjected to LPS, mice were treated with the iron chelator, deferoxamine (DFX). As shown in Fig. 7A, DFX (100 mg/kg) was administered i.p. once a day for 6 consecutive days. On the last day, LPS was also administered and different sickness-related behavioral tests were assessed, alongside with different biochemical analysis. DFX was able to reduce labile iron (Fig. 7B) and restore the iron metabolism alterations induced by LPS (Fig. 7C and D). Furthermore, DFX decreased the expression of pro-inflammatory markers such as iNOS and p65, though not CD68 (Fig. 7E and F) and the inflammasome-related markers NLRP3, caspase-1 and mature IL-1β (Fig. 7G and H). In addition, DFX also reduced the production of TNF-α and IL-1β cytokines (Fig. 7I). Moreover, DFX improved mice performance in the sickness behavioral tasks (Fig. 7J and K) and was able to decrease mice weight loss (Fig. S4D). The fact that DFX was able to restore most of the alterations observed in aged mice treated with LPS indicates that iron overload, possibly as a consequence of LPS-dependent microglial HO-1 overexpression, is related to the inflammation, oxidative stress and cognitive impairments observed in aged WT mice.

4. Discussion

This study demonstrates that microglial HO-1 depletion in aged mice exposed to an inflammatory challenge has positive effects by a mechanism that implicates the reduction of iron deposits in the brain. This finding contraposes the general idea that HO-1 induction could provide beneficial effects due to its antioxidant and anti-inflammatory properties, and highlights the importance of establishing a tight regulation of this enzyme.

The induction of HO-1 has been proposed as a potential strategy to

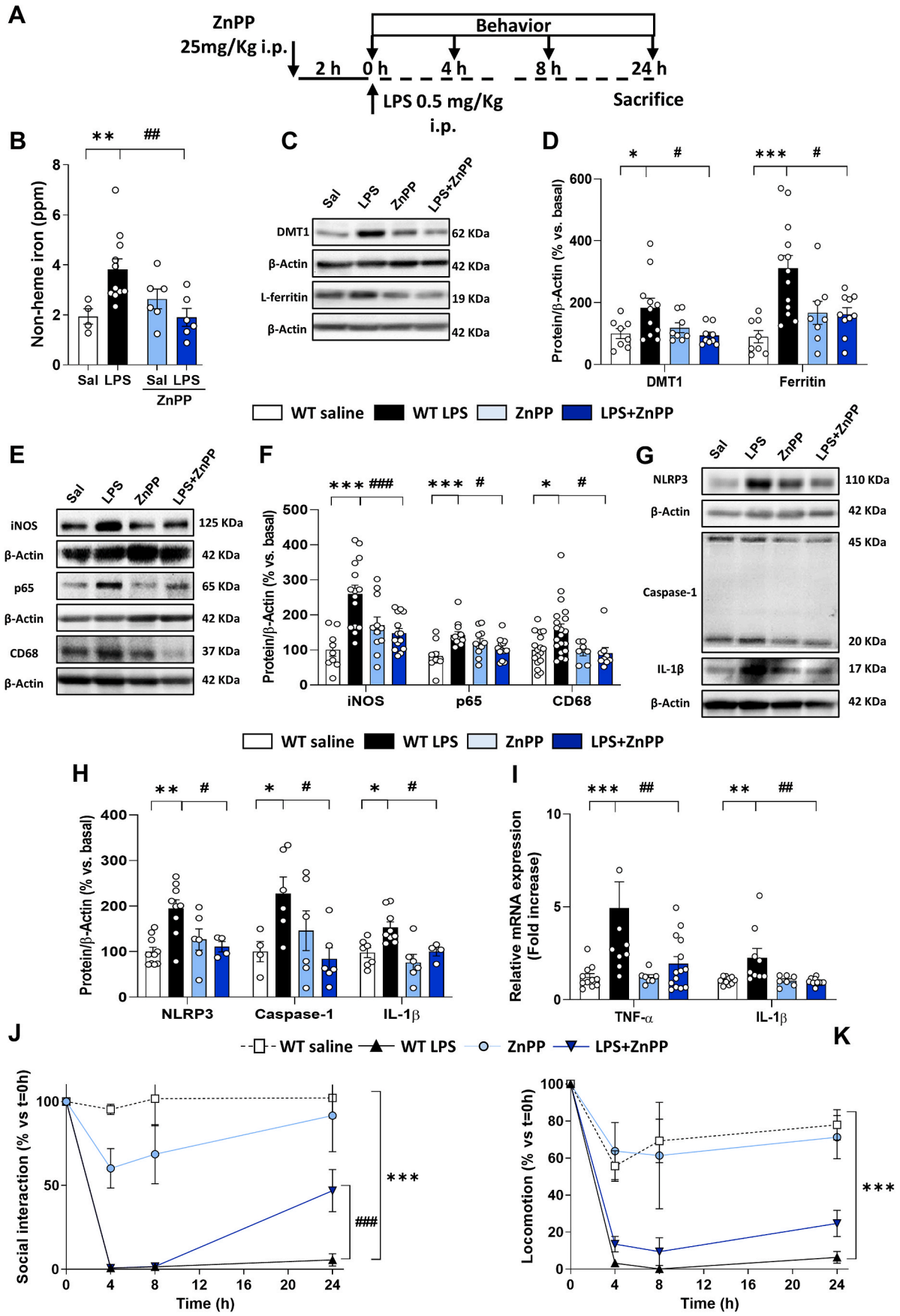

(caption on next page)

Fig. 6. Pharmacological inhibition of HO-1 activity with zinc protoporphyrin (ZnPP) reproduces a similar pattern to that observed in microglial HO-1 knock-out mice. (**A**) Scheme of the protocol followed. Mice were treated with ZnPP (25 mg/kg) 2 h prior the LPS (0.5 mg/kg) injection. ZnPP restored the iron metabolism alterations induced by LPS evidenced by a decrease in non-heme iron accumulation in the brain (**B**) and in the expression of DMT1 and L-ferritin in hippocampus (**C** and **D**). In a similar pattern to the genetic microglial depletion of HO-1, pharmacological inhibition reduced the inflammatory markers iNOS, p65 and CD68 in hippocampus (**E** and **F**), and was also able to revert the LPS-related increased expression of inflammasome-related proteins such as NLRP3, caspase-1 and mature IL-1 β, **(G** and **H)**. LPS-related increase in the pro-inflammatory cytokines TNF-α and IL-1β (**I**) was restored in WT mice treated with ZnPP. Treatment with ZnPP partially improved social interaction (**J**) and a statistical trend was observed for locomotion (**K**). Data represent mean ± S.E.M. (N = 4–20, one-way ANOVA followed by Tukey post-hoc test). Significant differences were considered when: *p < 0.05, **p < 0.01 and ***p < 0.001 compared to aged WT saline mice or #p < 0.05, ##p < 0.01 and ###p < 0.001 compared to aged WT LPS injected mice (**B–I**). Data represent mean ± S.E.M. (N = 5–15, 2-way ANOVA followed by Tukey post-hoc test). Significant differences were considered when: ***p < 0.001 compared to aged WT saline mice or ###p < 0.001 compared to aged WT LPS injected mice (**J-K**).

treat various NDDs [16,18,56,57]. However, there is still controversy regarding the role of HO-1 in aging and NDDs. In this study, we demonstrate that HO-1 is overexpressed in old mice (Fig. 1), but such increase is further enhanced when mice are peripherally challenged with a pro-inflammatory stimulus (LPS). This agrees with the finding that inflammatory insults in the periphery of the elder population cause low-grade neuroinflammation and induce brain HO-1 expression [8,9].

HO-1 catabolizes the heme group into CO, biliverdin/bilirubin and iron. On one hand, CO and bilirubin have anti-inflammatory, antioxidant and neuroprotective properties [16,17] while iron is an essential nutrient for the correct functioning of the brain as it is involved in neuronal respiration, myelin synthesis, production of neurotransmitters, synaptic plasticity and metabolic activities. In fact, $HMOX1^{-/-}$ mice (lack HO-1 in all cell types) exhibit microcytic anemia and iron redistribution and accumulation due to the inability of HO-1 deficient CD163+ phagocytes to degrade heme released from phagocyted erythrocytes and, consequently, this population of macrophages die [58]. CD163 is a scavenger receptor for the hemoglobin (Hb)-haptoglobin complex present in macrophages and microglia, which is critical for Hb clearance and heme catabolism [59]. In order to elucidate if $HMOX1^{M\text{-}KO}$ are devoid of CD163+ macrophage/microglia populations and develop microcytic anemia, different hematological parameters and CD163 levels were measured (Table S1 and figs. S2 and S5). In accordance to the literature [52], $HMOX1^{M\text{-}KO}$ mice did not develop microcytic anemia and had normal white blood cell counts (WBC) (Table S1 and Fig. S2). Furthermore, CD163 levels in $HMOX1^{M\text{-}KO}$ brain and spleen remained unchanged in comparison to WT (Fig. S5). These results suggest that under physiological conditions, $HMOX1^{M\text{-}KO}$ mice do not develop any of the iron-related abnormalities present in the total $HMOX1^{-/-}$ mice.

On the other hand, accumulation of labile iron is noxious as it participates in the *Fenton Reaction* generating oxygen radicals, promoting OS and leading to neuronal death [35–37]. It can therefore be hypothesized that if HO-1 is found chronically overexpressed, as it occurs with aging, and if it is further induced by an inflammatory challenge, rather than being beneficial it could be deleterious. Our results demonstrate that an inflammatory environment in aged mice increases the levels of non-heme iron in the brain by a mechanism related to augmented expression of iron import proteins (DMT1) and decreased expression of proteins related to iron export (FPN1), leading to iron accumulation. These results are in concordance with those that found that increases in labile iron in the aged brain were linked to a dysregulation in the expression of DMT1 and L-Ferritin [35,41]. Furthermore, in NDDs such as AD and PD, iron overload found in glial cells was related to an increase in DMT1 and hepcidin expression, a decrease in FPN1 and up-regulation of HO-1 [36,60,61]. Our results show that brain iron overload and iron metabolism alterations are linked to HO-1, specifically in microglia, as these alterations were significantly reverted in the $HMOX1^{M\text{-}KO}$ mice (Fig. 2). This is in line with other studies in which, under inflammatory conditions, iron accumulation was mostly found in microglia and, to a lesser extent, in astrocytes [34]. Moreover, microglial HO-1 is increased close by Aβ plaques and neurofibrillary tangles (NFT) in human AD samples, where Fe^{2+} deposits are found [62,63].

Iron accumulation causes a specific type of cell death known as ferroptosis, which is related to accumulation of lipid hydroperoxides and reduced levels of GPX4 [43–45,64]. In NDDs it has been hypothesized that iron deposits and thus, ferroptosis, are mainly regulated by the nuclear factor (erythroid-derived 2)-like 2 (NRF2)/HO-1 signaling pathway as NRF2 regulates GPX4 and HO-1 to induce iron intracellular accumulation [65]. In this line, our results evidence that an inflammatory stimulus in aged mice can cause ferroptosis as it generates iron overload, increases OS, and reduces GPX4 expression, leading to cognitive decline. Interestingly, these alterations were dependent on microglial HO-1, as in $HMOX1^{M\text{-}KO}$ mice we observed a decrease in iron deposits and in ferroptosis, as GPX4 levels were restored to saline levels. Moreover, this could explain the improvement in the recognition memory (Fig. 3H), which correlates with the report that links GPX4 depletion in neurons to cognitive impairment and neurodegeneration [64].

Our results indicate that LPS-dependent up-regulation of HO-1 leads to iron accumulation. In fact, after an endotoxic shock, the increase in labile iron coincides with the increase in HO-1 expression, rather than with the expression of iron metabolism-related proteins, such as ferroportin [66]. Therefore, iron released from microglia overexpressing HO-1 could be involved not only in the generation of OS, cell death and cognitive decline, but also favoring the proinflammatory response. This is in line with our results, where LPS prompted a shift in the microglial phenotype into a "primed" one [67], characterized by a higher release of proinflammatory cytokines (Fig. 4E) and induced sickness behavior in control aged mice (Fig. 4F and G) [12,14]. Interestingly, all these alterations were restored in $HMOX1^{M\text{-}KO}$ mice treated with LPS which relates HO-1 overexpression with neuroinflammation. Therefore, neuroinflammation and iron seem to be tightly regulated, as an inflammatory environment is related to iron accumulation and iron accumulation is linked to NDDs and neuroinflammation [36,54]. However, as previously mentioned, neuroinflammation leads to a reduction in ferroportin and an increase in hepcidin and DMT1 in the hippocampus, resulting in increased uptake and reduced export of iron [34]. Therefore, the observed effects could be independent of microglial HO-1-derived labile iron accumulation and microglial HO-1 might be acting indirectly, through inhibition of the inflammatory response. This idea is supported by the fact that HO-1 loss in macrophages is able to reduce systemic metainflammation by a mechanism that involves blunted NF-κB signaling. This agrees with our results, where $HMOX1^{M\text{-}KO}$ exhibit a reduction in p65, a subunit of NF-κB, iNOS, and the cytokines IL-1β and TNF-α, which are regulated by NF-κB signaling pathway. Moreover, HO-1 is required for metabolic programming, which may influence macrophage/microglial phenotype switch and thus systemic inflammation [52]. In fact, CD68, a marker of microglial switch into a more active state, was decreased in $HMOX1^{M\text{-}KO}$ mice treated with LPS. Therefore, microglial HO-1 loss could be acting by a mechanism that involves a reduction in neuroinflammation resulting in the restoration of LPS-dependent iron metabolism alterations in the brain.

Interestingly, total HO-1 pharmacological inhibition with ZnPP provided a similar outcome as with specific microglial HO-1 depletion in the $HMOX1^{M\text{-}KO}$ mice, which stresses the pivotal role of microglial HO-1 in regulating iron metabolism in the brain. Taken together, these results suggest that compounds able to inhibit HO-1 activity could be of interest

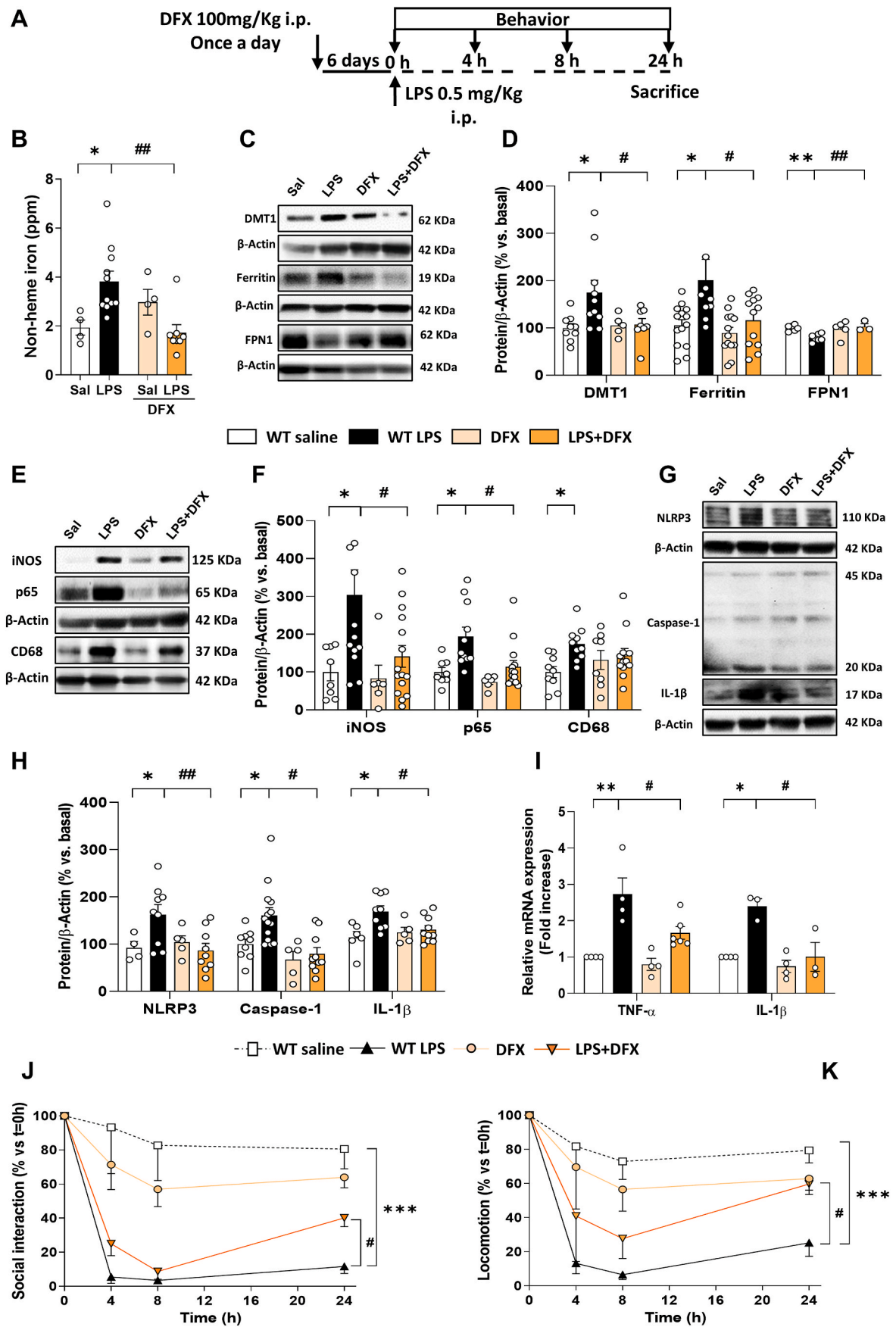

(caption on next page)

Fig. 7. Deferoxamine treatment improves the iron, inflammatory and behavioral alterations observed in aged mice challenged with LPS. (A) Schematic representation of the protocol. Mice were treated i.p. with DFX (100 mg/kg) once a day for 6 consecutive days. On the last day, DFX was administered followed by LPS (0.5 mg/kg) injection. DFX, was able to reduce the LPS-dependent non-heme iron accumulation in the brain (**B**) and to restore to basal levels the iron-related metabolism alterations, measured as changes in DMT1, L-ferritin and FPN1 in the hippocampus (**C** and **D**). DFX also decreased the expression of pro-inflammatory proteins, such as iNOS and p65 although it was not able to restore CD68 levels (**E** and **F**). Moreover, DFX was able to decrease the expression of inflammasome-related markers: NLRP3, caspase-1 and mature IL-1β (**G** and **H**) and reduced the mRNA levels of the pro-inflammatory cytokines TNF-α and IL-1β (**I**) in hippocampus. In addition, DFX treatment was able to partially restore sickness-behavioral alterations induced by LPS, measured as social interaction (**J**) and locomotion (**K**). Data represent mean ± S.E.M. (N = 3–15, one-way ANOVA followed by Tukey post-hoc test). Significant differences were considered when: *$p < 0.05$ and **$p < 0.01$ compared to aged WT saline mice or #$p < 0.05$ and ##$p < 0.01$ compared to aged WT LPS injected mice (**B–I**). Data represent mean ± S.E.M. (N = 4–11, two-way ANOVA followed by Tukey post-hoc test). Significant differences were considered when: ***$p < 0.001$ compared to aged WT saline mice or #$p < 0.05$ compared to aged WT LPS injected mice (**J-K**).

in NDDs as they potentially avoid iron overload, inflammation, neurodegeneration and cognitive decline. Related to this assumption, novel HO-1 inhibitors have provided neurotherapeutic effects in an AD animal model [68].

Finally, to support that LPS-dependent HO-1 upregulation was causing iron accumulation we used the iron chelator DFX. Iron chelators such as DFX or deferiprone have been tested in several NDDs mouse models such as PD, traumatic brain injury, intracerebral hemorrhage or Huntington's disease, with promising results [69,70]. In addition, there are several clinical trials, in which DFX or similar iron-chelators, as deferiprone, have been evaluated for different neurological diseases [71–73]. In relation to animal models of endotoxemia, DFX has also showed to exert neuroprotective and anti-neuroinflammatory properties [54,74]. The mechanism of action of DFX is related to its capacity to chelate iron and to decrease the expression of iron importers (DMT1), iron storage proteins (Fn) and to increase the levels of the iron exporter FPN1 [54,74]. Our results showed that DFX treatment prevented neuroinflammation (Fig. 7E–I) and restored iron metabolism alterations (Fig. 7B–D), which translated into behavioral improvements (Fig. 7J and K). Altogether, these results clearly indicate that microglial HO-1 overexpression was causing toxic accumulation of iron.

Our results support the idea that unregulated microglial HO-1 overexpression in the brain leads to iron accumulation, neuroinflammation and neurodegeneration. Therefore, a tight and controlled modulation of microglial HO-1 is needed in order to achieve beneficial outcomes from its activity. As $HMOX1^{M\text{-}KO}$ mice also lack HO-1 in macrophages and monocytes, and taking into account that ZnPP and DFX do not readily cross the blood brain barrier (BBB), a systemic regulation of the observed effects cannot be discarded [75]. In this scenario, myeloid HO-1 depletion, HO-1 inhibition by ZnPP and DFX-dependent iron chelation, could be linked to a reduction in labile iron in the periphery, a diminution in its leakage through the BBB, a lower recruitment of inflammatory cells and microglial activation. Although that is a possibility, direct effects of HO-1 loss or activity inhibition in the brain need to be considered as $HMOX1^{M\text{-}KO}$ mice do efficiently lack HO-1 in microglia (Fig. S1). Moreover, it has been reported that LPS and aging induce BBB hyperpermeability, favoring ZnPP to reach the brain and be locally inhibiting HO-1 activity. In fact, systemic ZnPP administration has been reported to improve brain injury in ICH and ischemia mouse models, where the BBB is disrupted [30,76–78]. In addition, there is evidence showing that after repeated systemic injections, DFX can penetrate the BBB and is found in significant quantities in different brain regions [79–82].

5. Conclusions

With aging, HO-1 is predominantly overexpressed in microglial cells and is further augmented under inflammatory conditions leading to iron accumulation, ferroptosis and behavioral deficits. However, genetic microglial HO-1 depletion, pharmacological inhibition of HO-1 activity or iron chelators provide beneficial effects on all the above-mentioned parameters, suggesting the role of microglial HO-1 in the iron-related pathological alterations and progression of inflammatory-related diseases. Therefore, strategies aiming to block HO-1 activity or moderate iron chelators could be interesting therapeutic approaches to reduce age-related pathological hallmarks and retard neurodegenerative disease progression.

Declaration of competing interest

Manuela García López, as corresponding author of Manuscript Ref. **REDOX-D-20-00255** and, on behalf of all co-authors (Cristina Fernández-Mendívil, Enrique Luengo, Paula Trigo-Alonso, Nuria García-Magro, Pilar Negredo), declares that the authors **have no conflict of interest**.

Acknowledgments

This study was supported by the Spanish Ministry of Economy and Competence Ref. RTI2018-095793-B-I00 to MGL and General Council for Research and Innovation of the Community of Madrid and European Structural Funds Ref. B2017/BMD-3827 – NRF24ADCM to M.G.L. C.F-M. and P.T-A have a fellowship from the Spanish Ministry of Science, Innovation and Universities (Ref. FPU15/03269 and Ref. FPU16/03239). E.L has a fellowship from Fundación Tatiana Pérez de Guzmán el Bueno. We would also like to thank María Dolores Vallejo from the Confocal Unit of the Universidad Autónoma de Madrid, Iliana Mir from the Animal Facilities of the Universidad Autónoma de Madrid, the Fundación Teófilo Hernando for its continuous support and all the lab members. We would like to thank BioRender for allowing us to generate the graphical abstract created with BioRender.com.

Appendix A. Supplementary data

Supplementary data to this article can be found online at https://doi.org/10.1016/j.redox.2020.101789.

Author's contributions

M.G.L. and C.F-M. conceived and designed the experiments. C.F-M., E.L, P.T-A and N.G-M performed the experiments. M.G.L and P.N. provided the resources and supervised the research. M.G.L. and C.F-M. wrote the manuscript. E.L, P.T-A, N.G-M and P.N reviewed and edited the manuscript.

References

[1] R.H. LeBlanc 3rd, R. Chen, M.H. Selim, K.A. Hanafy, Heme oxygenase-1-mediated neuroprotection in subarachnoid hemorrhage via intracerebroventricular deferoxamine, J. Neuroinflammation 13 (1) (2016) 244.
[2] T. Wyss-Coray, Ageing, neurodegeneration and brain rejuvenation, Nature 539 (7628) (2016) 180–186.
[3] J. Stephenson, E. Nutma, P. van der Valk, S. Amor, Inflammation in CNS neurodegenerative diseases, Immunology 154 (2) (2018) 204–219.
[4] R.M. Ransohoff, How neuroinflammation contributes to neurodegeneration, Science 353 (6301) (2016) 777–783.
[5] R.M. Barrientos, M.M. Kitt, L.R. Watkins, S.F. Maier, Neuroinflammation in the normal aging hippocampus, Neuroscience 309 (2015) 84–99.
[6] L.E.B. Bettio, L. Rajendran, J. Gil-Mohapel, The effects of aging in the hippocampus and cognitive decline, Neurosci. Biobehav. Rev. 79 (2017) 66–86.

[7] R. Olivieri, M. Michels, B. Pescador, P. Avila, M. Abatti, L. Cucker, et al., The additive effect of aging on sepsis-induced cognitive impairment and neuroinflammation, J. Neuroimmunol. 314 (2018) 1–7.
[8] T.K. Vo, P. Godard, M. de Saint-Hubert, G. Morrhaye, E. Bauwens, F. Debacq-Chainiaux, et al., Transcriptomic biomarkers of human ageing in peripheral blood mononuclear cell total RNA, Exp. Gerontol. 45 (3) (2010) 188–194.
[9] T.K. Vo, P. Godard, M. de Saint-Hubert, G. Morrhaye, C. Swine, V. Geenen, et al., Transcriptomic biomarkers of the response of hospitalized geriatric patients with infectious diseases, Immun. Ageing 7 (2010) 9.
[10] C. Mecca, I. Giambanco, R. Donato, C. Arcuri, Microglia and aging: the role of the TREM2-DAP12 and CX3CL1-CX3CR1 axes, Int. J. Mol. Sci. 19 (1) (2018).
[11] S. Hickman, S. Izzy, P. Sen, L. Morsett, J. El Khoury, Microglia in neurodegeneration, Nat. Neurosci. 21 (10) (2018) 1359–1369.
[12] Q. Li, B.A. Barres, Microglia and macrophages in brain homeostasis and disease, Nat. Rev. Immunol. 18 (4) (2018) 225–242.
[13] E.E. Spangenberg, K.N. Green, Inflammation in Alzheimer's disease: lessons learned from microglia-depletion models, Brain Behav. Immun. 61 (2017) 1–11.
[14] D.M. Norden, P.J. Trojanowski, F.R. Walker, J.P. Godbout, Insensitivity of astrocytes to interleukin 10 signaling following peripheral immune challenge results in prolonged microglial activation in the aged brain, Neurobiol. Aging 44 (2016) 22–41.
[15] S.L. Valles, A. Iradi, M. Aldasoro, J.M. Vila, C. Aldasoro, J. de la Torre, et al., Function of glia in aging and the brain diseases, Int. J. Med. Sci. 16 (11) (2019) 1473–1479.
[16] M. Nitti, S. Piras, L. Brondolo, U.M. Marinari, M.A. Pronzato, A.L. Furfaro, Heme oxygenase 1 in the nervous system: does it favor neuronal cell survival or induce neurodegeneration? Int. J. Mol. Sci. 19 (8) (2018).
[17] H.M. Schipper, W. Song, A. Tavitian, M. Cressatti, The sinister face of heme oxygenase-1 in brain aging and disease, Prog. Neurobiol. 172 (2019) 40–70.
[18] M. Bhardwaj, R. Deshmukh, M. Kaundal, B.V. Krishna Reddy, Pharmacological induction of hemeoxygenase-1 activity attenuates intracerebroventricular streptozotocin induced neurocognitive deficit and oxidative stress in rats, Eur. J. Pharmacol. 772 (2016) 43–50.
[19] H.M. Schipper, W. Song, H. Zukor, J.R. Hascalovici, D. Zeligman, Heme oxygenase-1 and neurodegeneration: expanding frontiers of engagement, J. Neurochem. 110 (2) (2009) 469–485.
[20] M.A. Smith, R.K. Kutty, P.L. Richey, S.D. Yan, D. Stern, G.J. Chader, et al., Heme oxygenase-1 is associated with the neurofibrillary pathology of Alzheimer's disease, Am. J. Pathol. 145 (1) (1994) 42–47.
[21] H. Tong, X. Zhang, X. Meng, L. Lu, D. Mai, S. Qu, Simvastatin inhibits activation of NADPH oxidase/p38 MAPK pathway and enhances expression of antioxidant protein in Parkinson disease models, Front. Mol. Neurosci. 11 (2018) 165.
[22] Y. Masaki, Y. Izumi, A. Matsumura, A. Akaike, T. Kume, Protective effect of Nrf2-ARE activator isolated from green perilla leaves on dopaminergic neuronal loss in a Parkinson's disease model, Eur. J. Pharmacol. 798 (2017) 26–34.
[23] A.A. Chora, P. Fontoura, A. Cunha, T.F. Pais, S. Cardoso, P.P. Ho, et al., Heme oxygenase-1 and carbon monoxide suppress autoimmune neuroinflammation, J. Clin. Invest. 117 (2) (2007) 438–447.
[24] N. Schallner, R. Pandit, R. LeBlanc 3rd, A.J. Thomas, C.S. Ogilvy, B.S. Zuckerbraun, et al., Microglia regulate blood clearance in subarachnoid hemorrhage by heme oxygenase-1, J. Clin. Invest. 125 (7) (2015) 2609–2625.
[25] E. Zeynalov, Z.A. Shah, R.C. Li, S. Dore, Heme oxygenase 1 is associated with ischemic preconditioning-induced protection against brain ischemia, Neurobiol. Dis. 35 (2) (2009) 264–269.
[26] H.M. Schipper, W. Song, A heme oxygenase-1 transducer model of degenerative and developmental brain disorders, Int. J. Mol. Sci. 16 (3) (2015) 5400–5419.
[27] W. Song, M. Cressatti, H. Zukor, A. Liberman, C. Galindez, H.M. Schipper, Parkinsonian features in aging GFAP.HMOX1 transgenic mice overexpressing human HO-1 in the astroglial compartment, Neurobiol. Aging 58 (2017) 163–179.
[28] M. Cressatti, W. Song, A.Z. Turk, L.R. Garabed, J.A. Benchaya, C. Galindez, et al., Glial HMOX1 expression promotes central and peripheral alpha-synuclein dysregulation and pathogenicity in parkinsonian mice, Glia 67 (9) (2019) 1730–1744.
[29] W. Song, V. Kothari, A.M. Velly, M. Cressatti, A. Liberman, M. Gornitsky, et al., Evaluation of salivary heme oxygenase-1 as a potential biomarker of early Parkinson's disease, Mov. Disord. 33 (4) (2018) 583–591.
[30] Z. Zhang, Y. Song, Z. Zhang, D. Li, H. Zhu, R. Liang, et al., Distinct role of heme oxygenase-1 in early- and late-stage intracerebral hemorrhage in 12-month-old mice, J. Cerebr. Blood Flow Metabol. 37 (1) (2017) 25–38.
[31] D. Wang, Y. Hui, Y. Peng, L. Tang, J. Jin, R. He, et al., Overexpression of heme oxygenase 1 causes cognitive decline and affects pathways for tauopathy in mice, J Alzheimers Dis 43 (2) (2015) 519–534.
[32] M. Cortes, M. Cao, H.L. Liu, C.S. Moore, L.D. Durosier, P. Burns, et al., alpha7 nicotinic acetylcholine receptor signaling modulates the inflammatory phenotype of fetal brain microglia: first evidence of interference by iron homeostasis, Sci. Rep. 7 (1) (2017) 10645.
[33] L.F. Wang, K.K. Yokoyama, C.L. Lin, T.Y. Chen, H.W. Hsiao, P.C. Chiang, et al., Knockout of ho-1 protects the striatum from ferrous iron-induced injury in a male-specific manner in mice, Sci. Rep. 6 (2016) 26358.
[34] V. Puy, W. Darwiche, S. Trudel, C. Gomila, C. Lony, L. Puy, et al., Predominant role of microglia in brain iron retention in Sanfilippo syndrome, a pediatric neurodegenerative disease, Glia 66 (8) (2018) 1709–1723.
[35] R. Gozzelino, P. Arosio, Iron homeostasis in health and disease, Int. J. Mol. Sci. 17 (1) (2016).
[36] T.J. Huat, J. Camats-Perna, E.A. Newcombe, N. Valmas, M. Kitazawa, R. Medeiros, Metal toxicity links to alzheimer's disease and neuroinflammation, J. Mol. Biol. 431 (9) (2019) 1843–1868.
[37] T.A. Rouault, Iron metabolism in the CNS: implications for neurodegenerative diseases, Nat. Rev. Neurosci. 14 (8) (2013) 551–564.
[38] R.C. McCarthy, J.C. Sosa, A.M. Gardeck, A.S. Baez, C.H. Lee, M. Wessling-Resnick, Inflammation-induced iron transport and metabolism by brain microglia, J. Biol. Chem. 293 (20) (2018) 7853–7863.
[39] R. Holland, A.L. McIntosh, O.M. Finucane, V. Mela, A. Rubio-Araiz, G. Timmons, et al., Inflammatory microglia are glycolytic and iron retentive and typify the microglia in APP/PS1 mice, Brain Behav. Immun. 68 (2018) 183–196.
[40] M.V. Rosato-Siri, L. Marziali, M.E. Guitart, M.E. Badaracco, M. Puntel, F. Pitossi, et al., Iron availability compromises not only oligodendrocytes but also astrocytes and microglial cells, Mol. Neurobiol. 55 (2) (2018) 1068–1081.
[41] L.N. Lu, Z.M. Qian, K.C. Wu, W.H. Yung, Y. Ke, Expression of iron transporters and pathological hallmarks of Parkinson's and alzheimer's diseases in the brain of young, adult, and aged rats, Mol. Neurobiol. 54 (7) (2017) 5213–5224.
[42] A.A. Belaidi, A.I. Bush, Iron neurochemistry in Alzheimer's disease and Parkinson's disease: targets for therapeutics, J. Neurochem. 139 (Suppl 1) (2016) 179–197.
[43] B.R. Stockwell, J.P. Friedmann Angeli, H. Bayir, A.I. Bush, M. Conrad, S.J. Dixon, et al., Ferroptosis: a regulated cell death Nexus linking metabolism, redox biology, and disease, Cell 171 (2) (2017) 273–285.
[44] Z. Zhang, Y. Wu, S. Yuan, P. Zhang, J. Zhang, H. Li, et al., Glutathione peroxidase 4 participates in secondary brain injury through mediating ferroptosis in a rat model of intracerebral hemorrhage, Brain Res. 1701 (2018) 112–125.
[45] G. Morris, M. Berk, A.F. Carvalho, M. Maes, A.J. Walker, B.K. Puri, Why should neuroscientists worry about iron? The emerging role of ferroptosis in the pathophysiology of neuroprogressive diseases, Behav. Brain Res. 341 (2018) 154–175.
[46] J.P. Godbout, J. Chen, J. Abraham, A.F. Richwine, B.M. Berg, K.W. Kelley, et al., Exaggerated neuroinflammation and sickness behavior in aged mice following activation of the peripheral innate immune system, Faseb. J. 19 (10) (2005) 1329–1331.
[47] M. Leger, A. Quiedeville, V. Bouet, B. Haelewyn, M. Boulouard, P. Schumann-Bard, et al., Object recognition test in mice, Nat. Protoc. 8 (12) (2013) 2531–2537.
[48] R. Wang, L. Liu, H. Liu, K. Wu, Y. Liu, L. Bai, et al., Reduced NRF2 expression suppresses endothelial progenitor cell function and induces senescence during aging, Aging (N Y) 11 (17) (2019) 7021–7035.
[49] H. Zukor, W. Song, A. Liberman, J. Mui, H. Vali, C. Fillebeen, et al., HO-1-mediated macroautophagy: a mechanism for unregulated iron deposition in aging and degenerating neural tissues, J. Neurochem. 109 (3) (2009) 776–791.
[50] B. Bellaver, D.G. Souza, D.O. Souza, A. Quincozes-Santos, Hippocampal astrocyte cultures from adult and aged rats reproduce changes in glial functionality observed in the aging brain, Mol. Neurobiol. 54 (4) (2017) 2969–2985.
[51] C. Fernández-Mendívil, M.M. Arreola, L.A. Hoshfield, K.N. Green, M.G. Lopez, Aging and progression of beta-amyloid pathology in Alzheimer's disease correlates with microglial heme-oxygenase-1 overexpression, Antioxidants 9 (7) (2020).
[52] A. Jais, E. Einwallner, O. Sharif, K. Gossens, T.T. Lu, S.M. Soyal, et al., Heme oxygenase-1 drives metaflammation and insulin resistance in mouse and man, Cell 158 (1) (2014) 25–40.
[53] S. Tzima, P. Victoratos, K. Kranidioti, M. Alexiou, G. Kollias, Myeloid heme oxygenase-1 regulates innate immunity and autoimmunity by modulating IFN-beta production, J. Exp. Med. 206 (5) (2009) 1167–1179.
[54] Y. Li, K. Pan, L. Chen, J.L. Ning, X. Li, T. Yang, et al., Deferoxamine regulates neuroinflammation and iron homeostasis in a mouse model of postoperative cognitive dysfunction, J. Neuroinflammation 13 (1) (2016) 268.
[55] S. Hong, V.F. Beja-Glasser, B.M. Nfonoyim, A. Frouin, S. Li, S. Ramakrishnan, et al., Complement and microglia mediate early synapse loss in Alzheimer mouse models, Science 352 (6286) (2016) 712–716.
[56] E. Parada, I. Buendia, E. Navarro, C. Avendano, J. Egea, M.G. Lopez, Microglial HO-1 induction by curcumin provides antioxidant, antineuroinflammatory, and glioprotective effects, Mol. Nutr. Food Res. 59 (9) (2015) 1690–1700.
[57] E. Navarro, I. Buendia, E. Parada, R. Leon, P. Jansen-Duerr, H. Pircher, et al., Alpha7 nicotinic receptor activation protects against oxidative stress via heme-oxygenase I induction, Biochem. Pharmacol. 97 (4) (2015) 473–481.
[58] G. Kovtunovych, M.A. Eckhaus, M.C. Ghosh, H. Ollivierre-Wilson, T.A. Rouault, Dysfunction of the heme recycling system in heme oxygenase 1-deficient mice: effects on macrophage viability and tissue iron distribution, Blood 116 (26) (2010) 6054–6062.
[59] A.J. Thomas, C.S. Ogilvy, C.J. Griessenauer, K.A. Hanafy, Macrophage CD163 expression in cerebrospinal fluid: association with subarachnoid hemorrhage outcome, J. Neurosurg. 131 (1) (2018) 47–53.
[60] J. Huo, Q. Cui, W. Yang, W. Guo, LPS induces dopamine depletion and iron accumulation in substantia nigra in rat models of Parkinson's disease, Int. J. Clin. Exp. Pathol. 11 (10) (2018) 4942–4949.
[61] M.S. Thomsen, M.V. Andersen, P.R. Christoffersen, M.D. Jensen, J. Lichota, T. Moos, Neurodegeneration with inflammation is accompanied by accumulation of iron and ferritin in microglia and neurons, Neurobiol. Dis. 81 (2015) 108–118.
[62] C. Cheignon, M. Tomas, D. Bonnefont-Rousselot, P. Faller, C. Hureau, F. Collin, Oxidative stress and the amyloid beta peptide in Alzheimer's disease, Redox Biol 14 (2018) 450–464.
[63] H.M. Schipper, S. Cisse, E.G. Stopa, Expression of heme oxygenase-1 in the senescent and Alzheimer-diseased brain, Ann. Neurol. 37 (6) (1995) 758–768.
[64] W.S. Hambright, R.S. Fonseca, L. Chen, R. Na, Q. Ran, Ablation of ferroptosis regulator glutathione peroxidase 4 in forebrain neurons promotes cognitive impairment and neurodegeneration, Redox Biol 12 (2017) 8–17.

[65] X. Song, D. Long, Nrf2 and ferroptosis: a new research direction for neurodegenerative diseases, Front. Neurosci. 14 (2020) 267.
[66] J.C. Duvigneau, C. Piskernik, S. Haindl, B. Kloesch, R.T. Hartl, M. Huttemann, et al., A novel endotoxin-induced pathway: upregulation of heme oxygenase 1, accumulation of free iron, and free iron-mediated mitochondrial dysfunction, Lab. Invest. 88 (1) (2008) 70–77.
[67] S.M. O'Neil, K.G. Witcher, D.B. McKim, J.P. Godbout, Forced turnover of aged microglia induces an intermediate phenotype but does not rebalance CNS environmental cues driving priming to immune challenge, Acta Neuropathol Commun 6 (1) (2018) 129.
[68] A. Gupta, B. Lacoste, P.J. Pistell, D.K. Ingram, E. Hamel, M.A. Alaoui-Jamali, et al., Neurotherapeutic effects of novel HO-1 inhibitors in vitro and in a transgenic mouse model of Alzheimer's disease, J. Neurochem. 131 (6) (2014) 778–790.
[69] C. Guo, T. Wang, W. Zheng, Z.Y. Shan, W.P. Teng, Z.Y. Wang, Intranasal deferoxamine reverses iron-induced memory deficits and inhibits amyloidogenic APP processing in a transgenic mouse model of Alzheimer's disease, Neurobiol. Aging 34 (2) (2013) 562–575.
[70] J.M. Fine, A.C. Forsberg, D.B. Renner, K.A. Faltesek, K.G. Mohan, J.C. Wong, et al., Intranasally-administered deferoxamine mitigates toxicity of 6-OHDA in a rat model of Parkinsons disease, Brain Res. 1574 (2014) 96–104.
[71] G. Grolez, C. Moreau, B. Sablonniere, G. Garcon, J.C. Devedjian, S. Meguig, et al., Ceruloplasmin activity and iron chelation treatment of patients with Parkinson's disease, BMC Neurol. 15 (2015) 74.
[72] D. Devos, C. Moreau, J.C. Devedjian, J. Kluza, M. Petrault, C. Laloux, et al., Targeting chelatable iron as a therapeutic modality in Parkinson's disease, Antioxidants Redox Signal. 21 (2) (2014) 195–210.
[73] G. Cossu, G. Abbruzzese, G. Matta, D. Murgia, M. Melis, V. Ricchi, et al., Efficacy and safety of deferiprone for the treatment of pantothenate kinase-associated neurodegeneration (PKAN) and neurodegeneration with brain iron accumulation (NBIA): results from a four years follow-up, Park. Relat. Disord. 20 (6) (2014) 651–654.
[74] X.Y. Zhang, J.B. Cao, L.M. Zhang, Y.F. Li, W.D. Mi, Deferoxamine attenuates lipopolysaccharide-induced neuroinflammation and memory impairment in mice, J. Neuroinflammation 12 (2015) 20.
[75] P.A. Rodgers, D.S. Seidman, P.L. Wei, P.A. Dennery, D.K. Stevenson, Duration of action and tissue distribution of zinc protoporphyrin in neonatal rats, Pediatr. Res. 39 (6) (1996) 1041–1049.
[76] A. Zakaria, M. Rady, L. Mahran, K. Abou-Aisha, Pioglitazone attenuates lipopolysaccharide-induced oxidative stress, dopaminergic neuronal loss and neurobehavioral impairment by activating Nrf2/ARE/HO-1, Neurochem. Res. 44 (12) (2019) 2856–2868, https://doi.org/10.1007/s11064-019-02907-0.
[77] Y. Gong, H. Tian, G. Xi, R.F. Keep, J.T. Hoff, Y. Hua, Systemic zinc protoporphyrin administration reduces intracerebral hemorrhage-induced brain injury, Acta Neurochir. Suppl. 96 (2006) 232–236.
[78] P. Vannemreddy, A.K. Ray, R. Patnaik, S. Patnaik, S. Mohanty, H.S. Sharma, Zinc protoporphyrin IX attenuates closed head injury-induced edema formation, blood-brain barrier disruption, and serotonin levels in the rat, Acta Neurochir. Suppl. 96 (2006) 151–156.
[79] Y. Hua, R.F. Keep, J.T. Hoff, G. Xi, Deferoxamine therapy for intracerebral hemorrhage, Acta Neurochir. Suppl. 105 (2008) 3–6.
[80] H. Keberle, The biochemistry of desferrioxamine and its relation to iron metabolism, Ann. N. Y. Acad. Sci. 119 (1964) 758–768.
[81] C. Palmer, R.L. Roberts, C. Bero, Deferoxamine posttreatment reduces ischemic brain injury in neonatal rats, Stroke 25 (5) (1994) 1039–1045.
[82] C. Hershko, D.J. Weatherall, Iron-chelating therapy, Crit. Rev. Clin. Lab Sci. 26 (4) (1988) 303–345.